Journal of Materials Chemistry C

FEATURE ARTICLE

View Article Online
View Journal | View Issue

Cite this: J. Mater. Chem. C, 2014, 2, 6921

Received 13th May 2014
Accepted 16th June 2014

DOI: 10.1039/c4tc00988f

www.rsc.org/MaterialsC

Carbon quantum dots: synthesis, properties and applications

Youfu Wang and Aiguo Hu*

Carbon quantum dots (CQDs, C-dots or CDs), which are generally small carbon nanoparticles (less than 10 nm in size) with various unique properties, have found wide use in more and more fields during the last few years. In this feature article, we describe the recent progress in the field of CQDs, focusing on their synthetic methods, size control, modification strategies, photoelectric properties, luminescent mechanism, and applications in biomedicine, optronics, catalysis and sensor issues.

1. Introduction

Carbon-based quantum dots consisting of graphene quantum dots (QGDs) and carbon quantum dots (CQDs, C-dots or CDs) are a new class of carbon nanomaterials with sizes below 10 nm. They were first obtained during the purification of single-walled carbon nanotubes through preparative electrophoresis in 2004,[1] and then *via* laser ablation of graphite powder and cement in 2006.[2] Carbon-based quantum dots with fascinating properties have gradually become a rising star as a new nanocarbon member due to their benign, abundant and inexpensive nature.[3] Carbon is commonly a black material, and was generally considered to have low solubility in water and weak fluorescence. Wide attention has been focused on carbon-based quantum dots because of their good solubility and strong luminescence, for which they are referred to as carbon nanolights.[3]

During the past few years, much progress has been achieved in the synthesis, properties and applications of carbon-based quantum dots, as reviewed by Baker *et al.*,[3] Lee *et al.*,[4] and Zhu *et al.*[5] Compared to traditional semiconductor quantum dots and organic dyes, photoluminescent carbon-based quantum dots are superior in terms of high (aqueous) solubility, robust chemical inertness, facile modification and high resistance to photobleaching. The superior biological properties of carbon-based quantum dots, such as low toxicity and good biocompatibility, entrust them with potential applications in bioimaging, biosensor and biomolecule/drug delivery. The outstanding electronic properties of carbon-based quantum dots as electron donors and acceptors, causing chemiluminescence and electrochemical luminescence, endow them with wide potentials in optronics, catalysis and sensors.

Shanghai Key Laboratory of Advanced Polymeric Materials, School of Materials Science and Engineering, East China University of Science and Technology, Shanghai, 200237, China. E-mail: hagmhsn@ecust.edu.cn; Fax: +86-21-64253037; Tel: +86-21-64253037

Youfu Wang was born in Anqing City, Anhui province of China. He received his B.Sc. degree from East China University of Science and Technology (ECUST, China) in 2011. Then, he was admitted to pursue his Ph.D. degree in ECUST under the supervision of Professor Aiguo Hu. His current research focuses on synthetic polymer chemistry and rationally designed carbon nanomaterials for electronic applications.

Aiguo Hu received his Ph.D. degree from Nankai University in 2001 (with Prof. Jitao Wang). After working as postdoctoral fellow in the University of North Carolina at Chapel Hill (USA) (with Prof. Wenbin Lin), he returned to China and kicked off his independent research at ECUST in 2007. He was promoted as an "Eastern Scholar Professor" in 2011. His main research interests are synthetic polymer chemistry, functional nanostructure, rationally designed carbon materials for electronic applications, and functionalized polymers for pharmaceutical applications.

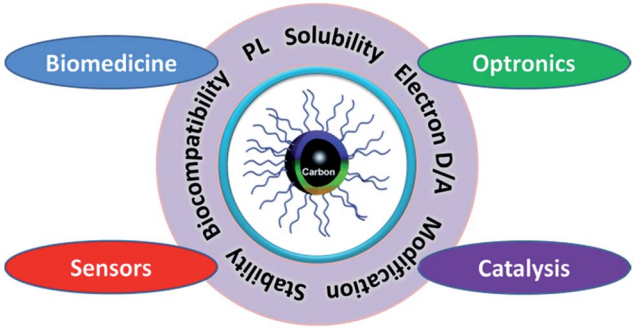

Fig. 1 CQDs with unique properties have great potential in biomedicine, optronics, catalysis and sensors.

As the properties and applications of GQDs have been systematically summarized elsewhere,[5–7] we will focus our horizons on CQDs due to their unique properties and great potential in various applications (Fig. 1). In this feature article, we describe the recent progress in the field of CQDs, focusing on their synthetic methods, size control, modification strategies, optical properties, luminescent mechanism, and applications in biomedicine, optronics, catalysis and sensor issues.

2. Synthesis, size control and modification

Many methods have been proposed to prepare CQDs during the last decade, which can be roughly classified into "Top-down" and "Bottom-up" approaches, and they can be modified during preparation or post-treatment (Fig. 2). Three problems facing CQDs preparation need to be noticed: (i) carbonaceous aggregation during carbonization, which can be avoided by using electrochemical synthesis, confined pyrolysis or solution chemistry methods, (ii) size control and uniformity, which is important for uniform properties and mechanistic study, and can be optimized *via* post-treatment, such as gel electrophoresis, centrifugation, and dialysis and (iii) surface properties that are critical for solubility and selected applications, which can be tuned during preparation or post-treatment. We will discuss the main methods for CQDs synthesis, the size control *via* confined pyrolysis and the modification of CQDs, including functionalization, doping and nanohybrids. The features of different synthetic methods for the preparation of CQDs are summarized in Table 1.

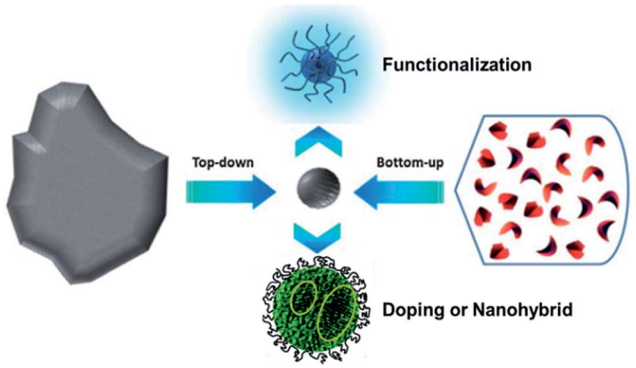

Fig. 2 Schematic illustration of CQDs preparation *via* "top-down" and "bottom-up" approaches, and modification including functionalization, doping and nanohybrids. Adapted with permission.[8] Copyright 2013, Royal Society of Chemistry.

2.1. Synthetic methods

2.1.1. Chemical ablation. Strong oxidizing acids carbonize small organic molecules to carbonaceous materials, which can be further cut into small sheets by controlled oxidation.[9–14] This method may suffer from harsh conditions and drastic processes. Peng and Travas-Sejdic reported a simple route to prepare luminescent CQDs in an aqueous solution by dehydrating carbohydrates with concentrated H_2SO_4, followed by breaking the carbonaceous materials into individual CQDs with HNO_3, and finally passivating with amine-terminated compounds (4,7,10-trioxa-1,13-tridecanediamine).[13] The surface passivation was essential for the photoluminescence (PL) of these CQDs. The emission wavelength of these CQDs can be tuned by differing the starting material and the duration of the nitric acid treatment. The multicolor emission capabilities and nontoxic nature of these CQDs enable them to be applied in life science research.

Photoluminescent CQDs were synthesized in one-pot using polyethylenimine (PEI), a cationic branched polyelectrolyte, as both a carbon source and passivating agent *via* HNO_3 oxidation.[14] In contrast to the commonly reported pH-insensitive CQDs, the PL of these CQDs was highly pH-sensitive, *i.e.*, the PL intensity decreased with increasing pH from pH 2 to 12. In addition, the pH response of the PL behaviour was reversible. This property endows them the potential to serve as proton sensors in monitoring cell metabolization processes with proton release. When incubated with HeLa cells, the CQDs could readily penetrate the cell membrane and exhibit low cytotoxicity and favorable biocompatibility, which is essential for HeLa cell imaging.

2.1.2. Electrochemical carbonization. Electrochemical soaking is a powerful method to prepare CQDs using various bulk carbon materials as precursors.[15–21] However, there are only a few reports about electrochemically carbonizing small molecules to CQDs. Preparation of CQDs *via* the electrochemical carbonization of low-molecular-weight alcohols is proposed by Zhang and co-workers.[22] Two Pt sheets were used as the working and auxiliary electrode, and a calomel electrode mounted on a freely adjustable Luggin capillary was used as the reference electrode. The alcohols were transformed into CQDs after electrochemical carbonization under basic conditions.[21] The sizes and graphitization degrees of these CQDs increase with the increasing applied potential. The resultant CQDs with amorphous core exhibited excellent excitation- and size-dependent PL properties without complicated purification and passivation procedures. Note that the quantum yields (QYs) of these CQDs can reach 15.9%. CQDs can be prepared from different small molecular alcohols showing low toxicity to human cancer cells.

Table 1 The features of the different synthetic methods used for the preparation of CQDs

Synthetic Methods	Advantages	Disadvantages	Ref.
Chemical ablation	Most accessible, various sources	Harsh conditions, drastic processes, multiple-steps, poor control over sizes	9–14
Electrochemical carbonization	Size and nanostructure are controllable, stable, one-step	Few small molecule precursors	15–22
Laser ablation	Rapid, effective, surface states tunable	Low QY, poor control over sizes, modification is needed	2 and 23–27
Microware irradiation	Rapid, scalable, cost effective, eco-friendly	Poor control over sizes	28–31
Hydrothermal/solvothermal treatment	Cost effective, eco-friendly, non-toxic	Poor control over sizes	34–40

2.1.3. Laser ablation. Sun and co-workers produced CQDs *via* laser ablation of a carbon target in the presence of water vapour with argon as a carrier gas at 900 °C and 75 kPa.[2,23–27] After refluxing in HNO_3 for 12 h and passivating the surface by attaching simple organic species such as PEG_{1500N} (amine-terminated polyethylene glycol) and poly(propionylethyleneimine-*co*-ethyleneimine) (PPEI-EI),[23,25] the acid-treated CQDs gave bright luminescence emission. Du *et al.* reported the synthesis of fluorescent CQDs by laser irradiation of a suspension of carbon materials in an organic solvent (Fig. 3).[23] By selecting organic solvents, the surface states of the CQDs could be modified to achieve tunable light emission. Based on control experiments, the origin of the luminescence was attributed to the surface states related to the ligands on the surface of the CQDs. Li *et al.* reported a simple laser ablation approach to prepare CQDs using nano-carbon materials as the starting material and a simple solvent as the liquid media.[24] In a typical procedure, 0.02 g of nano-carbon material was dispersed in 50 mL of solvent (such as ethanol, acetone, or water). After ultrasonication, 4 mL of the suspension was dropped into a glass cell for laser irradiation. A Nd:YAG pulsed laser with a second harmonic wavelength of 532 nm was used to irradiate the suspension. After laser irradiation, the solution was centrifuged to obtain the supernatant containing the CQDs.

2.1.4. Microwave irradiation. Microwave irradiation of organic compounds is a rapid and low-cost method to synthesize CQDs.[28–31] Using sucrose as the carbon source and diethylene glycol (DEG) as the reaction media, green luminescent CQDs were obtained within one minute under microwave irradiation.[30] These DEG-stabilized CQDs (DEG-CQDs) could be well-dispersed in water with a transparent appearance. With an increase in the excitation wavelength, the intensity of the PL first increased to a maximum (360 nm excitation) and then decreased. However, no perceptible shift of the PL peak over an excitation range from 320 to 380 nm could be observed. Moreover, these DEG-CQDs could be efficiently ingested by C6 glioma cells and exhibited a low cytotoxicity, suggesting their potential in bioimaging. Liu *et al.* promoted microwave-mediated pyrolysis of citric acid with various amine molecules to synthesize highly luminescent CQDs.[29] The amine molecules, especially primary amine molecules, play dual function as N-doping precursors and surface passivating agents for the CQDs, which enhanced the PL performance. The QY values greatly increased with an increase in N content for the CQDs fabricated from citric acid and 1,2-ethylenediamine, showing a QY up to 30.2%. The resultant CQDs are highly biocompatible and have great potential for biomedical applications.

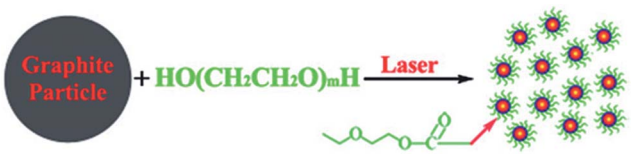

Fig. 3 A one-step synthesis of CQDs in PEG_{200N} solvent *via* laser irradiation. Adapted with permission.[23] Copyright 2009, Royal Society of Chemistry.

2.1.5. Hydrothermal/solvothermal treatment. Hydrothermal carbonization (HTC)[32,33] or solvothermal carbonization is a low cost, environmentally friendly, and nontoxic route to produce novel carbon-based materials from various precursors. Typically, a solution of organic precursor is sealed and reacted in a hydrothermal reactor at high temperature. CQDs were prepared *via* HTC from many precursors such as glucose,[34] citric acid,[35] chitosan,[36] banana juice,[37] and protein.[38] Mohapatra *et al.* prepared highly photoluminescent CQDs with a QY of 26% in one step by hydrothermal treatment of orange juice followed by centrifugation.[39] These CQDs with sizes of 1.5–4.5 nm were applied in bioimaging due to their high photostability and low toxicity. Liu *et al.* reported a one-step synthesis of amino-functionalized fluorescent CQDs by hydrothermal carbonization of chitosan at 180 °C for 12 hours.[36] Note that the amino-functionalized fluorescent CQDs can be used directly as novel bioimaging agents.

Solvothermal carbonization followed by extraction with an organic solvent is a popular approach to prepare CQDs.[40,41] Typically, carbon-yielding compounds were subjected to heat treatment in high boiling point organic solvents, followed by extraction and concentration. Bhunia *et al.* synthesized two kinds of the CQDs, hydrophobic and hydrophilic with diameters less than 10 nm from the carbonization of carbohydrates.[40] The hydrophobic ones were produced by mixing different amounts of carbohydrate with octadecylamine and octadecene before being heated up to 70–300 °C for 10–30 minutes. The hydrophilic ones can be synthesized by heating an aqueous solution of carbohydrate within wide pH ranges. The

hydrophilic CQDs with yellow and red emissions can also be synthesized by mixing an aqueous solution of carbohydrate with concentrated phosphoric acid followed with heating at 80–90 °C for 60 min (Fig. 4).

2.2. Size control-confined pyrolysis

For particular applications and mechanistic study, it is important to control the sizes of CQDs to get uniform properties. Many approaches have been proposed to obtain uniform CQDs during preparation or post-treatment. In most of the reports, the as-synthesized CQDs fragments were purified *via* post-treatments like filtration, dialysis, centrifugation, column chromatography and gel-electrophoresis. It is of great importance to control the size during the preparation process. Discrete CQDs with tunable and uniform sizes can be prepared *via* confined pyrolysis of an organic precursor in nanoreactors (Fig. 5). Three steps were used as follows: (i) absorbing the organic precursor into porous nanoreactors *via* capillary force, (ii) pyrolysis of the organic precursor confined in the nanoreactors into carbonaceous matter, (iii) release of the as-synthesized CQDs by removing the nanoreactors. The size and size-distribution of the CQDs produced from this method are dictated by the texture parameters of the nanoreactors.

Porous silicas are the most widely used nanoreactors for their various, tunable and easily obtained textures, thermal stability and easy removal.[43–45] Zhu *et al.* synthesized hydrophilic CQDs with mesoporous silica nanospheres as nanoreactors by impregnation of a citric acid precursor (Fig. 5).[5,45]

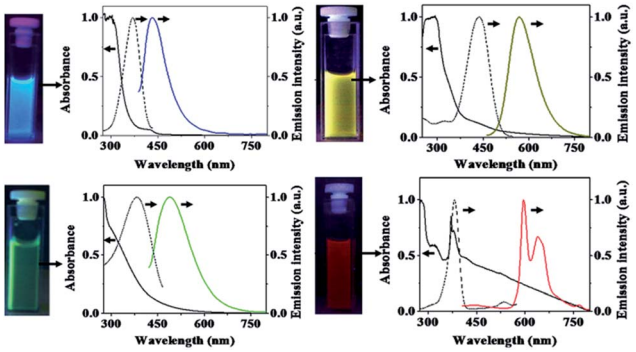

Fig. 4 Digital images of CQDs solutions under appropriate excitations and their absorption (solid black lines), excitation (dashed black lines) and emission (color lines) spectra. Emission spectra were measured by excitation at 370 nm, 400 nm, 425 nm, and 385 nm for CQD – blue, CQD – green, CQD – yellow, and CQD – red, respectively. All excitation spectra were recorded in respective emission maxima. Adapted with permission.[40] Copyright 2013, Nature Publishing Group.

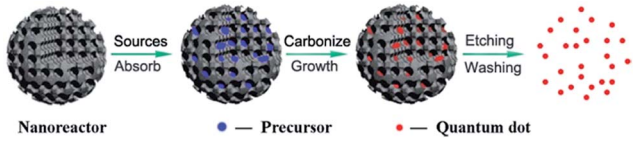

Fig. 5 Schematic illustration of the preparation of CQDs *via* confined pyrolysis of an organic precursor in nanoreactors. Adapted with permission.[5] Copyright 2012, Royal Society of Chemistry.

After pyrolysis at 300 °C for 2 hours in air, followed by silica removal and dialysis, CQDs with a uniform size of 1.5–2.5 nm were prepared and showed good photostability, low toxicity, excellent luminescence, and up-conversion properties.

Polymeric core–shell nanoparticles are also effective nanoreactors with thermally cross-linkable core and thermally removable shell.[42,46,47] Recently, we prepared CQDs *via* pyrolysis of PAN@PMMA core–shell nanoparticles prepared using a one-pot micro-emulsion polymerization process (Fig. 6).[42] The core PAN domain was crosslinked and chipped at 270 °C under air with protection from the shell PMMA domain. Furthermore, elevating the temperature caused the carbonization of the PAN fragments and decomposition of the PMMA domains to release the N-doped CQDs. The prepared CQDs showed dual emission at about 410 nm and 450 nm and stable PL in moderate pH solutions, which is essential for bioimaging.

Thermally unstable polymers are also used as block matter to avoid carbonaceous aggregation during thermal treatment, especially when the carbon-yielding domain is a cross-linkable polymer.[8,48] We prepared well-defined CQDs with tunable and uniform sizes from single-chain polymeric nanoparticles, which were formed using a Bergman cyclization-intermediated chain collapse[49–51] of linear polymers containing enediyne units (Fig. 7).[8] The polynaphthylene-containing polymeric nanoparticles formed were transformed to CQDs *via* a bijective way (one-to-one correspondence). The sizes of the final CQDs can be easily tuned by changing the length of the polymeric chains or the grafting degrees of the enediyne in each chain. The prepared CQDs showed size-dependant luminescent properties and the PL peak blue-shifted with an increase of size. The PL mechanism of CQDs was also investigated based on experimental results and theoretical simulation, and it will be discussed in detail in Section 3.2.

2.3. Surface functionalization

Surface modification is a powerful method to tune the surface properties of materials for selected applications. There are

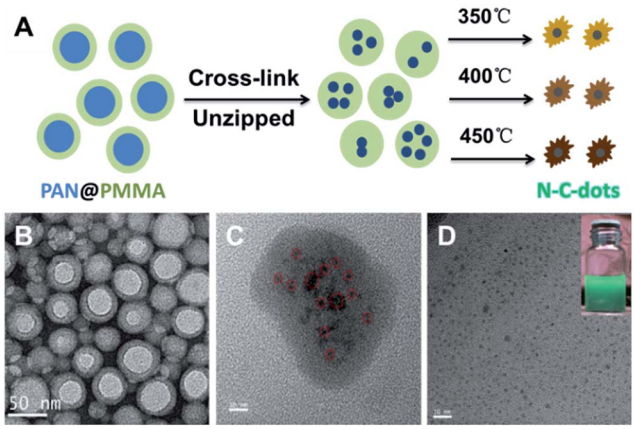

Fig. 6 Scheme of preparing CQDs from polymeric nanoparticles (A) and the TEM images of the core–shell polymeric nanoparticles (B), core cross-linked polymeric nanoparticles (C) and final CQDs (D). The digital image of the CQDs solution is shown in the inset. Adapted with permission.[42] Copyright 2013, Royal Society of Chemistry.

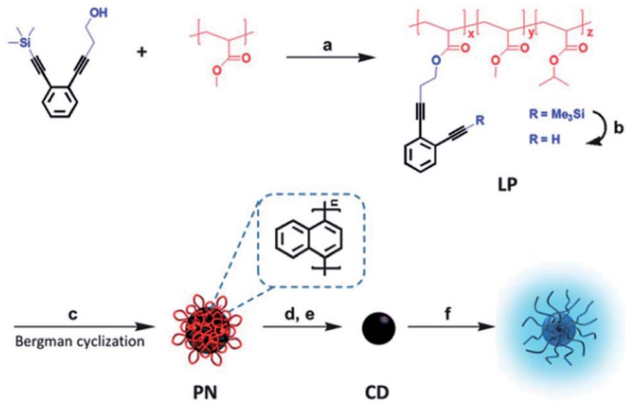

Fig. 7 Preparation of soluble CQDs with tunable sizes from single-chain polymeric nanoparticles. Adapted with permission.[8] Copyright 2013, Royal Society of Chemistry.

many approaches for functionalizing the surface of CQDs through the surface chemistry or interactions, such as covalent bonding,[36,52–54] coordination,[55] π–π interactions,[56] and sol–gel technology.[57,58]

The majority of CQDs are rich in oxygen-containing groups, which endows them with feasibility in covalent bonding. Surface passivation *via* covalent bonding of amine-containing agents is a common method to improve the PL of CQDs, which showed an important influence on the properties of CQDs. Fluorescent CQDs with diameters of about 3 nm emitting blue-green light were synthesized using a hydrothermal carbonization of 2Na·EDTA. Then, the CQDs were functionalized with spiropyrans to obtain surface-functionalized CQDs. The emission of the functionalized CQDs centered at 510 nm could be switched off, while being turned on at 650 nm *via* energy transfer between the CQDs and spiropyrans after irradiation with ultraviolet (UV) light (Fig. 8).[59] The process could be reversed using irradiation with visible light. The functionalized CQDs show excellent photo-reversibility and high stability.

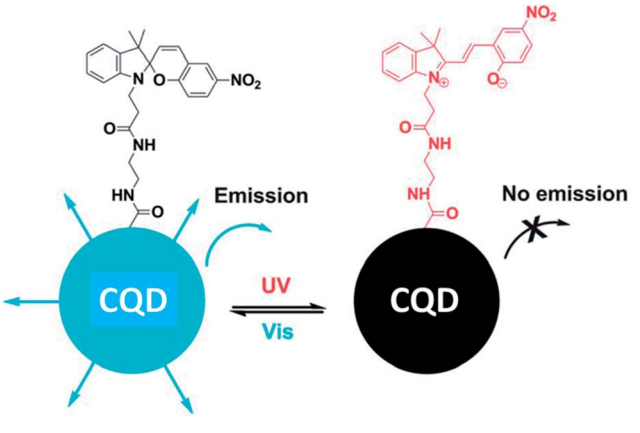

Fig. 8 Schematic illustration of the light-induced fluorescence modulation of spiropyran-functionalized CQDs. Adapted with permission.[59] Copyright 2013, Royal Society of Chemistry.

In addition to covalent bonding to CQDs, coordination is another useful strategy. A simple method for phosphate (Pi) detection (Fig. 9) was established by developing an off-on fluorescence probe using europium-adjusted CQDs, which was successfully applied to the detection of Pi in complicated matrixes such as an artificial wetlands system.[55] When the surface carboxyl groups on the CQDs were coordinated with Eu^{3+}, the fluorescence of the CQDs was turned off. The fluorescence can, however, be switched on when Eu^{3+} was specifically coordinated with Pi.

The Sol–gel technique is also a promising approach for decorating the surface of CQDs with functional molecules. Liu *et al.* reported a method to synthesize highly luminescent (QY = 47%) amorphous CQDs in one minute using organo-silane as a coordinating solvent.[57] The CQDs, benefited from the surface methoxysilyl groups, have a diameter of ~0.9 nm and can easily be fabricated into pure CQDs fluorescent films or monoliths by simply heating at 80 °C for 24 h. Moreover, the water-insoluble CQDs can be further transformed into water-soluble CQDs/silica particles with good biocompatibility and low toxicity. CQDs@MIP (molecularly imprinted polymer) was synthesized by a one-pot, room-temperature, sol–gel polymerization and was applied as a fluorescence sensor for the detection of dopamine in an aqueous solution.[58]

2.4. CQDs doping

Doping is a widely used approach to tune the PL properties of photoluminescent materials. Various doping methods with dozens of elements such as N,[35,36,41,42,60–62] S,[63,64] and P[65] have been reported to tune the properties of CQDs.

N-doping is the most studied way to enhance the emission of the CQDs by inducing an upward shift in the Fermi level and electrons in the conduction band.[66] It was demonstrated that only the nitrogen bonding to carbon can really enhance the PL emission of CQDs. The N-CQDs show nitrogen content-dependent PL intensities with multicolor and two-photon up-conversion properties.[29,41] A Mg/N co-doping strategy to fabricate highly luminescent CQDs with QY of 83% was studied by Liu *et al.* (Fig. 10).[67] After hydrothermal treatment of a homogeneous solution containing citric acid and $Mg(OH)_2$ at 200 °C for 3 h, the raw products were treated by filtration, dialysis and lyophilization to obtain CQDs denoted as Mg-CQDs. The Mg-citric acid chelate in the carbon source was utilized to introduce Mg and preserve the majority of the carboxyl groups, which

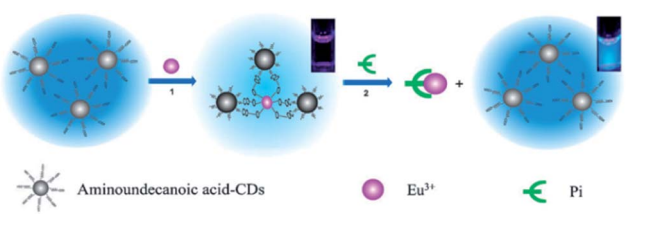

Fig. 9 Schematic representation of Pi detection based on the off-on fluorescence probe of CQDs adjusted by Eu^{3+}. Adapted with permission.[55] Copyright 2011, Royal Society of Chemistry.

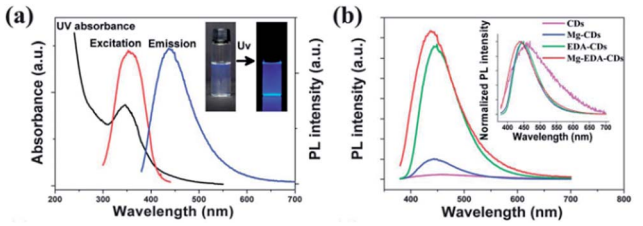

Fig. 10 (a) UV-Vis and PL spectra (λ_{ex} = 360 nm) of the Mg–EDA-CQDs in an aqueous solution (insets: photographs under natural light and UV light). (b) PL spectra (λ_{ex} = 360 nm) of CQDs with different doping strategies. Adapted with permission.[67] Copyright 2014, Royal Society of Chemistry.

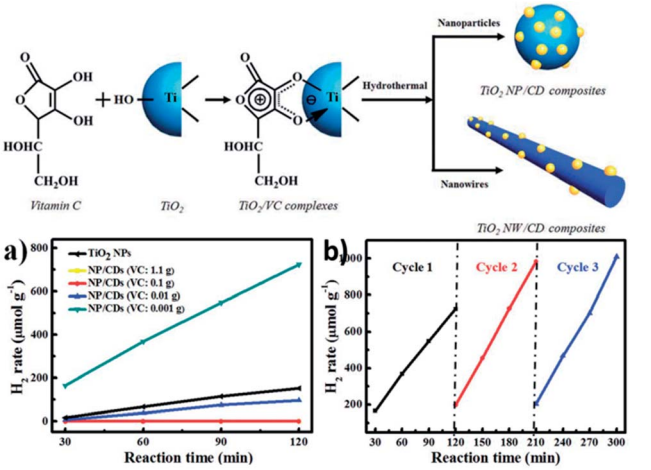

Fig. 11 (Up) Schematic illustration of the *in situ* hydrothermal synthesis of TiO_2/CQD nanohybrids. (Down) (a) Time course of H_2 production from TiO_2 NPs and NP/CQDs composites synthesized at different VC amounts: 1.1, 0.1, 0.01 and 0.001 g. (b) A typical time course of H_2 production from NP/CQDs composites for 3 cycles. Adapted with permission.[69] Copyright 2014, Royal Society of Chemistry.

together with the N-passivation contributed to a dramatic increase in the PL enhancement of the final CQDs.

P- and N-co-doped CQDs were synthesized *via* microwave irradiation of DMF in the presence of phosphoric acid.[65] These CQDs exhibited excellent photoluminescent characteristics with high electrocatalytic activity and good tolerance to the methanol crossover effects in the oxygen reduction reaction (ORR) in an alkaline medium due to heteroatom functionalization. Sulfur- and nitrogen-*co*-doped CQDs (S–N-CQDs) were synthesized on a large-scale using sulfuric acid to carbonize and etch hair fiber.[63] It was found that S and N can form different binding configurations in the S–N-CQDs framework, such as a –C–S– covalent bond of the thiophene-S and –C–SO_x– (x = 2, 3, 4, sulfate or sulfonate) for S-doped, pyridinic N and pyrrolic N for N-doped, respectively. Moreover, a higher reaction temperature leads to the formation of S–N-CQDs with smaller size, higher S content, and longer wavelength of photoluminescent emissions. The resultant S–N-CQDs also exhibited good luminescence stability, low toxicity, excellent biocompatibility, and high solubility.

2.5. CQDs nanohybrids

More recently, many efforts have been focused on the preparation of novel hybrids comprised of CQDs and inorganic nanoparticle cores (*e.g.*, iron oxide,[68] zinc oxide, silica,[21] and titania[21,69]). The resultant hybrids integrate the fluorescence properties of the CQDs with the magnetic, optical or mechanical properties of the oxide cores. Such hybrids hold great promise as magneto-optical biolabeling agents or efficient photocatalysts.

TiO_2/CQDs composites were synthesized *in situ* from bidentate TiO_2/vitamin-C (VC) complexes *via* a hydrothermal method.[69] The effects of the amounts of VC, hydrothermal temperatures and reaction times were explored for the H_2 generation from photocatalytic water splitting catalyzed by the TiO_2/CQDs nanohybrids. The TiO_2-NPs/CQDs nanohybrids obtained at 200 °C for 2 h with a VC amount of 0.001 g showed a 9.7-fold higher H_2 production rate than bare TiO_2 NPs and showed good cycling performance (Fig. 11). The TiO_2-NWs/CQDs nanohybrids prepared at 90 °C for 4 h also produced hydrogen at a rate of 1189.7 μmol g^{-1} h^{-1}, which is 4.2 times higher than that of bare TiO_2 NWs. The superior photocatalytic performance of these nanohybrids may be attributed to the synergetic effects of the hydrothermal treatment along with the favourable electron transfer ability and up conversion of the CQDs.

Au NPs were used to enhance the fluorescence of CQDs by forming Au-PAMAM-CQD conjugates using an amidation reaction.[70] In this process, PAMAM serves as a spacer of a suitable size to keep the Au NPs and CQDs at an appropriate distance from one another for PL enhancement. Both the amount of Au NPs and CQDs can influence the fluorescence enhancement. An appropriate amount of Au NPs and CQDs linked to PAMAM leads to an optimum fluorescence enhancement. The PL intensity of CQDs can be enhanced as much as 62-fold by conjugating Au NPs and CQDs with an optimized molar ratio to PAMAM, which is desirable for many applications.

3. Properties and luminescent mechanism

3.1. Optical properties

3.1.1. Adsorption. CQDs typically show optical absorption in the UV region with a tail extending to the visible range (see Fig. 12A (ref. 2) for representative spectra). There may be some absorption shoulders (Fig. 10a for an example) attributed to the π–π* transition of the C=C bonds, the n–π* transition of C=O bonds and/or others.

3.1.2. Fluorescence. One of the most fascinating features of CQDs, both from fundamental and application-oriented perspectives, is their PL (see Fig. 12 for representative spectra). In most cases of early study, one unique feature of the PL of CQDs was the clear λ_{ex} dependence of the emission wavelength and intensity. Whether this occurs because of optical selection of differently sized nanoparticles (quantum effect) and/or

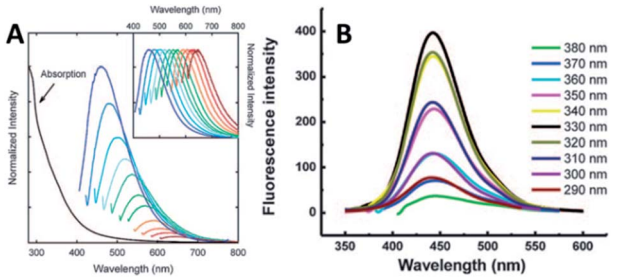

Fig. 12 (A) Absorbance and PL spectra with increasingly longer excitation wavelengths (in 20 nm increments starting from 400 nm) of 5 nm PPEI-EI CQDs in an aqueous solution formed using laser ablation methods (inset shows the normalized PL spectra). Adapted with permission.[2] Copyright 2006, American Chemical Society. (B) PL of 1.9 nm CQDs at different excitation wavelengths of 290–380 nm. Adapted with permission.[19] Copyright 2008, Royal Society of Chemistry.

different emissive traps on the CQDs surface or another mechanism is currently unresolved (Section 3.2). Moreover, the requirement for surface passivation is only partially understood, but appears to be linked to the synthetic method. However, more and more cases have emerged with an λ_{ex} independent emission position,[19,42,71] which may be attributed to their uniform size and surface chemistry.

The PL properties of the CQDs can be tuned *via* modification as described in Section 2 or *via* electron/energy transfer as demonstrated in Fig. 8 and Section 3.1.7.

3.1.3. Phosphorescence. The phosphorescence properties of CQDs were discovered recently. A pure organic room temperature phosphorescent (RTP) material was obtained based on water soluble CQDs and its phosphorescent lifetime was lengthened to the sub-second order (~380 ms).[72] By dispersing the CQDs into a polyvinyl alcohol (PVA) matrix, clear phosphorescence could be observed at room temperature when excited with UV light. Preliminary investigations suggested that the phosphorescence originated from the triplet excited states of aromatic carbonyls on the surface of the CQDs. The matrix PVA molecules can effectively protect the triplet excited state energy from rotational or vibrational loss by rigidifying these groups with hydrogen bonding (Fig. 13).

3.1.4. Chemiluminescence (CL). CL properties of CQDs were firstly discovered when the CQDs coexisted with some oxidants, such as potassium permanganate ($KMnO_4$) and cerium(IV).[73] The electron paramagnetic resonance (EPR) reveals that oxidants, such as $KMnO_4$ and cerium(IV), can inject holes into the CQDs. This process increases the population of the holes in the CQDs and accelerates the electron–hole annihilation, resulting in energy release in the form of CL emission. Moreover, the CL intensity was dependent on the concentration of the CQDs in a certain range. It was also found that increasing the temperature had a positive effect on the CL due to the thermal equilibrium of electron distribution in the CQDs as shown in Fig. 14. It is interesting for this system that the CL properties can be designed by changing their surface groups.[74]

A novel CL phenomenon was also observed for the as-prepared CQDs in a strong alkaline solution (NaOH or KOH).

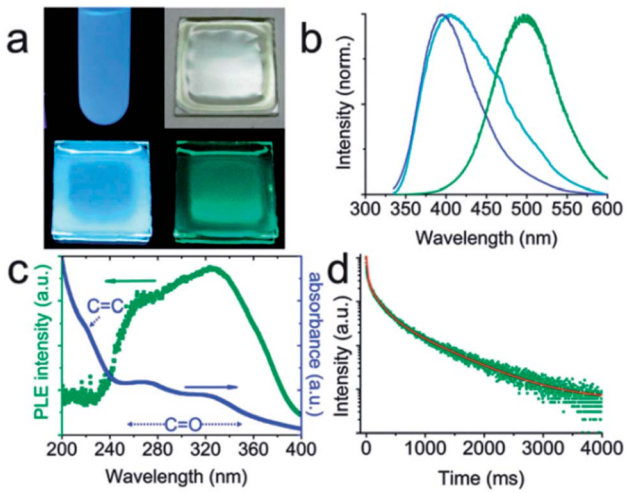

Fig. 13 (a and b) Digital photographs and the corresponding spectra of CQDs: dispersed in water under UV light (a: upper left; b: blue line); dispersed in a PVA matrix under daylight (a: upper right), UV light (a: lower left; b: cyan line) and right after UV light has been turned off (a: lower right; b: olive line). The UV excitation for the photographs is 365 nm, while that for the spectra is 325 nm. (c) Phosphorescence excitation spectrum (olive dots) and absorption spectrum (blue dots) of CQDs dispersed in water. (d) Time-resolved phosphorescence spectrum. Adapted with permission.[72] Copyright 2013, Royal Society of Chemistry.

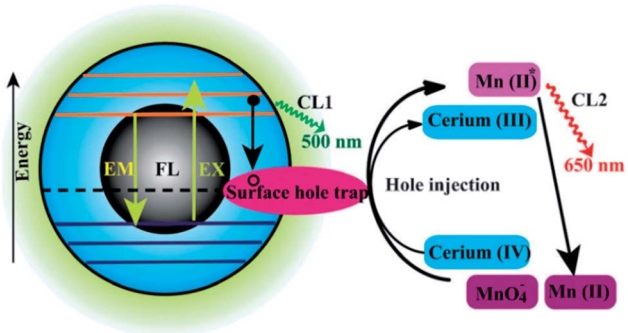

Fig. 14 Schematic illustration of the FL and CL mechanisms in the CQDs–$KMnO_4$ and CQDs–cerium(IV) systems. CL1 and CL2 represent two CL routes in the system. Adapted with permission.[73] Copyright 2012, Royal Society of Chemistry.

The CQDs exhibited excellent electron donor ability towards dissolved oxygen to form the superoxide anion radical ($O_2^{\bullet-}$) in a solution of NaOH. These results directly provided evidence for the excellent electron-donating ability of CQDs.[75,76] Radiative recombination of the injected electrons by "chemical reduction" of the CQDs and thermally excited generated holes was suggested to account for the CL behaviour in strong alkaline solutions.[76]

The CL of CQDs opens up new opportunities for their potential in the determination of reductive substances.[77] The dual role of CQDs as an electron donor and acceptor offers great potential in optronics and catalysis as described in Section 4.2 and 4.3.

3.1.5. Electrochemical luminescence (ECL). To understand how the composition, morphology, and surface structure of CQDs affects the PL and ECL in selected applications, CQDs with low and high oxidation levels, denoted as r-CQDs and o-CQDs, were synthesized *via* a carbonization–extraction strategy and carbonization–oxidation process, respectively.[78] The results showed that the electrochemical response was controlled by the diffusion of o-CQDs onto the electrode surface (Fig. 15B). The ECL wave started at 1.10 V and reached its peak value at 1.30 V (Fig. 15C), which is consistent with the oxidation peak in the cyclic voltammograms (CVs); thus, the ECL emission was related to the direct oxidization of o-CQDs. Fig. 15D shows the ECL under continuous cyclic scans with high reproducibility. The cathodic ECL of the o-CQDs/$K_2S_2O_8$ system is illustrated in Fig. 15B. The "loose shell" with oxygen-containing groups on the o-CQDs facilitates the electro-generation of o-CQDs radicals. The reduction of $S_2O_8^{2-}$ releases a strong oxidizing agent, the $SO_4^{\bullet -}$ radical, which accepts an electron from the anionic o-CQD$^{\bullet -}$ to form the emitters for ECL emission. The low ECL activity of r-CQDs also showed that the ECL is related to the oxidation state of the surface.

3.1.6. Up-conversion photoluminescence (UCPL). The UCPL properties of CQDs can be attributed to the multi-photon activation process, in which the simultaneous absorption of two or more photons leads to the emission of light at a shorter wavelength than the excitation wavelength (anti-Stokes type emission). The UCPL of CQDs opens up new opportunities for cell imaging with two-photon luminescence microscopy, as well as highly efficient catalyst design, for applications in bioscience and energy technology. Upon excitation in the NIR region, the PL spectra showed a fixed emission peak at 540 nm that did not shift with a variation of the excitation wavelength (Fig. 16B),[79] which was different from that previously reported (Fig. 16A).[45] The fixed emission position showed that the emission occurs from the lowest single state irrespective of the mode of excitation.

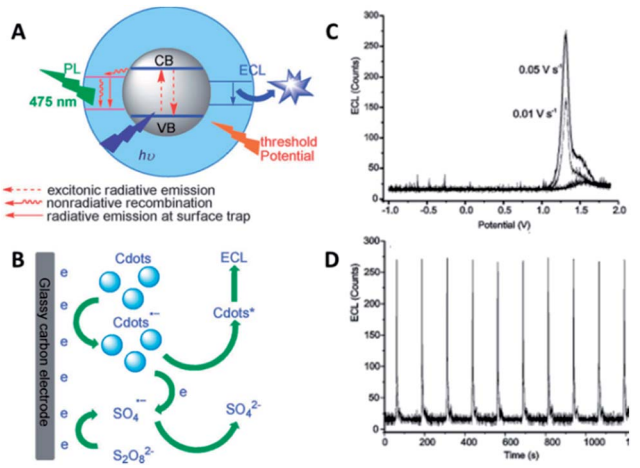

Fig. 15 (A) Schematic illustration of the PL and ECL emissions of CQDs. (B) The mechanism of ECL in the o-CQDs/$K_2S_2O_8$ system. (C) ECL profiles of o-CQDs at a scan rate of 0.01 and 0.05 V s^{-1}. (D) The reproducibility of ECL in a continuous scan mode. Adapted with permission.[78] Copyright 2013, Wiley-VCH.

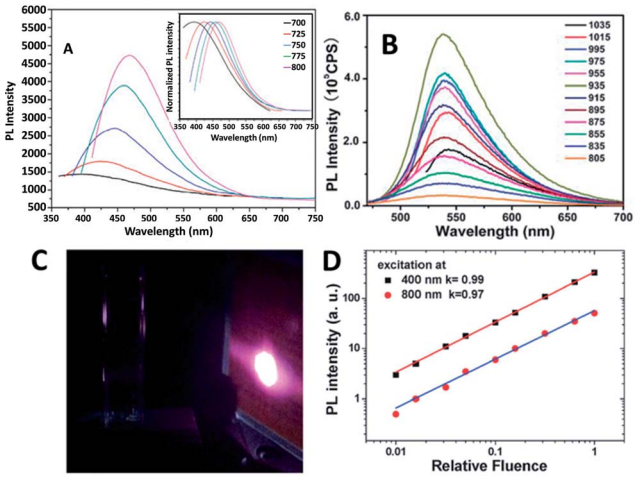

Fig. 16 (A) UCPL spectra of the CQDs dispersed in water at excitation wavelengths progressively increasing from 700 nm in 25 nm increments. Inset: the corresponding normalized PL spectra. Adapted with permission.[45] Copyright 2011, Royal Society of Chemistry. (B) UCPL properties of CQDs dispersed in water at excitation wavelengths from 805 nm to 1035 nm. Adapted with permission.[79] Copyright 2012, Royal Society of Chemistry. (C) The photographs of the CQD solution excited at 800 nm with 100 mW laser (the bright spot is laser on an infrared detection paper). (D) Excitation intensity dependence of fluorescence with excitation at 400 nm (black squares) and 800 nm (red circles) in a fluorescence spectrophotometer. Adapted with permission.[80] Copyright 2014, Royal Society of Chemistry.

The UCPL of CQDs is a fascinating feature, however, very recently, a UCPL study on five differently synthesized CQDs and GQDs demonstrated that the CQDs and GQDs did not exhibit observable UCPL.[80] Under the experimental conditions reported earlier, so-called UCPL in five differently synthesized CQDs and GQDs in a commercial fluorescence spectrophotometer was observed. However, the UCPL actually originates from the normal fluorescence excited by the leaking component from the second diffraction in the monochromator of the fluorescence spectrophotometer (Fig. 16C). The leaking component and thus UCPL can be eliminated by adding a suitable long-pass filter in the excitation pathway of a fluorescence spectrophotometer. Intensity dependent experiments clearly confirmed that the so-called UCPL is actually the normal fluorescence with linear response rather than a multiple phonon process (Fig. 16D). These experiments suggested that most of the CQDs and GQDs may not have detectable UCPL. Note that it is necessary to eliminate the normal fluorescence and measure the excitation intensity dependence of the fluorescence when observing UCPL of CQDs.

3.1.7. Photoinduced electron transfer (PET) property. For the utilization of PL compounds in light-energy conversion and related areas, there have been extensive investigations on their photoresponse, photoinduced charge separation and electron transfer processes.

Sun *et al.* found that the PL from a CQDs solution could be efficiently quenched in the presence of either electron acceptors such as 4-nitrotoluene and 2,4-dinitrotoluene or electron donors such as *N*,*N*-diethylaniline.[81] Namely, the photoexcited

CQDs are excellent as both electron donors and electron acceptors. They also found efficient PL quenching in CQDs by surface-doped metals through disrupting the excited state redox processes.[82] Electron transfer in nanocomposites of CQDs–GO, CQDs–MWNTs and CQDs–TiO_2 NPs without linker molecules was also studied.[83] Significant PL quenching was observed in the CQD–GO system, which was attributed to the ultrafast electron transfer from CQDs to GO with a time constant of 400 fs. In comparison, addition of carbon nanotubes resulted in static quenching of fluorescence in CQDs. No charge transfer was observed in either CQD–MWNT or CQD–TiO_2 nanocomposites. These interesting PET properties of CQDs as an electron donor/acceptor may offer new opportunities for light-energy conversion, catalysis and related applications, as well as mechanistic elucidation.

3.2. PL mechanism

Although there have been many efforts focused on the physicochemical properties of CQDs, the origin of the observed optoelectronic behaviour is a topic of discussion to date.

The origin of the PL of CQDs has been assigned to several reasons in the literature: optical selection of differently sized nanoparticles (quantum effect),[3,21] defects and surface states,[23] surface groups,[84] surface passivation,[3] fluorophores with different degrees of π-conjugation,[85,86] and the recombination of electron–hole pairs localized within small sp^2 carbon clusters embedded within a sp^3 matrix.[87]

A systematic investigation on the formation mechanism of the CQDs prepared from pyrolysis of citric acid (CA)–ethanolamine (EA) precursor at different temperatures was presented recently.[62] Pyrolysis at 180 °C leads to a CQD precursor with an intense PL and high QY formed by the dehydration of CA–EA. At higher temperatures (230 °C) a carbonaceous core starts to form. The PL at this stage is contributed from the presence of both molecular fluorophores and the carbonaceous core (Fig. 17). CQDs that exhibit mostly or exclusively PL arising from carbonaceous cores were obtained at even higher temperatures (300 and 400 °C, respectively). Since the molecular fluorophores predominate at low pyrolysis temperatures while the carbonaceous core starts forming at higher temperatures, the PL behaviour of CQDs strongly depends on the conditions used in their synthesis.

Multiple fluorescence intensity levels of individual CQDs were observed recently.[88] Imaging of single CQDs at different excitation energies revealed significant heterogeneity in the lower energy trap sites between particles. It is also found that individual CQDs exhibit single-step photobleaching and transient blinking to the background level suggesting single-molecular behaviour. These observations suggest the possibility that single CQDs can possess multiple chromophoric units associated with the CQDs core and oxygenated defect-related emissive traps. Interestingly, the majority of the reduced CQDs showed multiple levels, while the oxidized CQDs predominantly showed a single level. A possible reason for this is that after the initial excitation the energy is transferred from the higher energy absorbing site to a lower energy emissive site in the oxidized CQDs. In contrast, the low-energy emissive traps were entirely or partially removed when CQDs are reduced, blocking the energy-transfer pathways. Consequently, the emission for reduced CQDs is likely to be from the originally excited chromophores. The presence of the emissive traps or quenching states would likely be dependent on the synthetic methods and the post-treatment of CQDs.

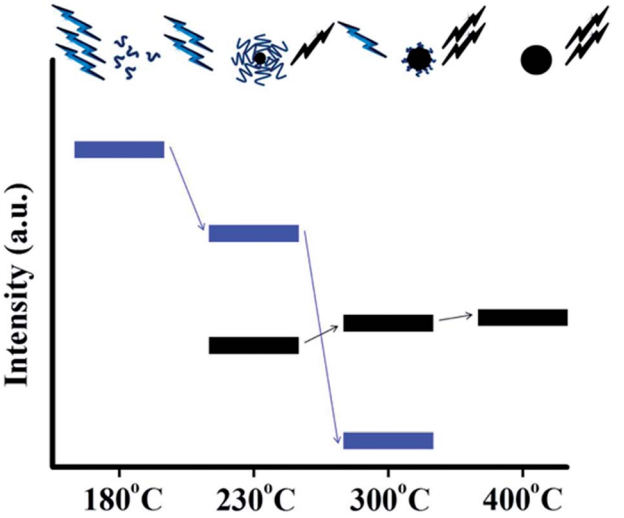

Fig. 17 Schematic representation of the emission characteristics of three photoactive species produced from the thermal treatment of a mixture of CA and EA. During pyrolysis, the organic fluorophores (blue groups) are consumed for the build-up of the carbonaceous core (black sphere) so that the PL component, which corresponds to the carbonaceous core (black bars), increases at the expense of the component that arises from the organic fluorophores (blue bars). Adapted with permission.[62] Copyright 2011, American Chemical Society.

Fig. 18 shows the optical images of CQDs of four typical sizes, illuminated by white and UV light, and the corresponding emission spectra from left to right.[21] The PL properties vary sensitively with the size of the CQDs (Fig. 18c), and with increasing size, the emissions were red-shifted. The theoretical calculations (Fig. 18d) showed the dependence of the HOMO–LUMO gap on the size of the graphene fragments. As the size of the fragment increases, the gap decreases gradually, and the gap energy in the visible spectral range was obtained from graphene fragments with a diameter of 14–22 Å, which agrees well with the visible emission of CQDs with diameters of <3 nm. Thus, it is deduced that the strong emission of CQDs comes from the quantum-sized graphite structure instead of the carbon–oxygen surface.

We recently prepared soluble CQDs with tunable sizes from single-chain polymeric nanoparticles (Fig. 7).[8] PL study shows that the optimal emission wavelength of CQDs is red-shifted when the size of CQDs decreases, which is different from the trends typically found in semiconductor quantum dots and CQDs prepared from graphitized materials.[21] To clarify the PL mechanism of CQDs prepared from different sources, a theoretical study based on density functional theory was performed. Two series of model compounds, fused aromatic rings and

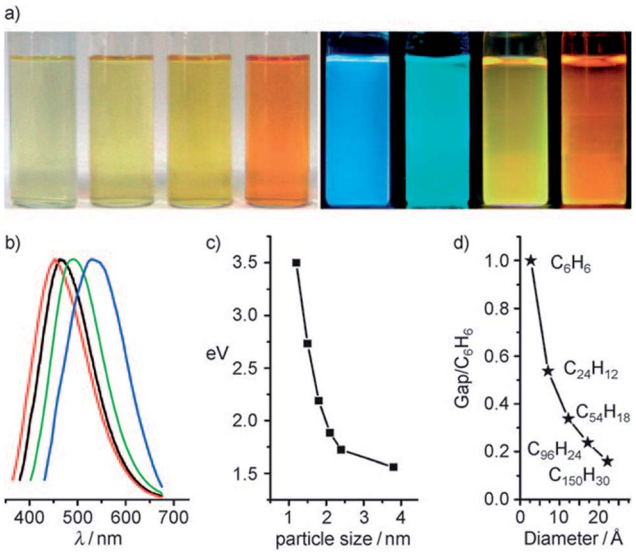

Fig. 18 (a) Typically sized CQDs optical images illuminated under white (left; daylight lamp) and UV light (right; 365 nm); (b) PL spectra of typically sized CQDs: the red, black, green, and blue lines are the PL spectra for blue-, green-, yellow-, and red-emission CQDs, respectively; (c) the relationship between the CQDs size and PL properties; (d) HOMO–LUMO gap dependence on the size of the graphene fragments. Adapted with permission.[21] Copyright 2010, Wiley-VCH.

cyclo-1,4-naphthylenes, were chosen for CQDs with different microstructures. The calculation data indicated that the PL energy of CQDs is dictated by the size and microstructure of the sp^2 carbon core. For CQDs with a graphitized core (Class I), the smaller the size of the core (Fig. 18c and d), the higher the PL energy, while for CQDs with an amorphous core (Class II), an inverse trend is observed (Fig. 19). CQDs exhibit a higher PL intensity after surface reduction but no obvious emission shift, which further shows that the QY of CQDs is controlled by the surface chemistry.[89]

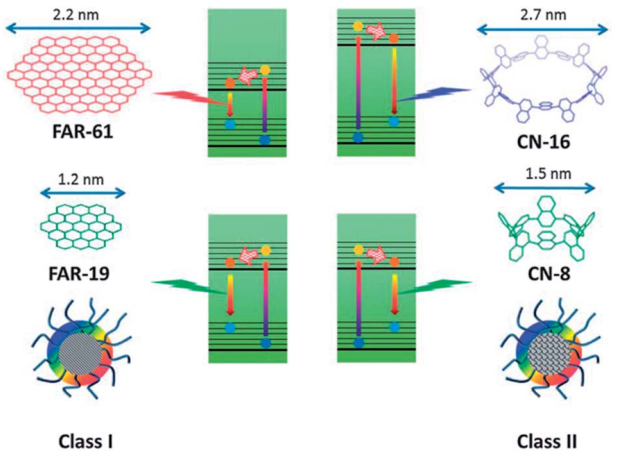

Fig. 19 Schematic illustration of the PL mechanism of Class I and Class II CQDs. Adapted with permission.[8] Copyright 2013, Royal Society of Chemistry.

CQDs synthesized by electrochemical ablation and small molecule carbonization, as well as GQDs fabricated by solvothermally cutting graphene oxide, are three typical green fluorescence carbon-based quantum dots. Ultrafast spectroscopy was used to investigate the PL origin in these fluorescent carbon-based quantum dots. According to the change of surface functional groups during chemical reduction and the obvious emission-type transformation, these green luminescence emissions are unambiguously assigned to special edge states consisting of several carbon atoms on the edge of carbon backbone and functional groups with C=O functionality (carbonyl and carboxyl groups).[90] These findings suggest that the competition among various emission centers (bright edge states) and traps dominate the optical properties of fluorescent carbon-based quantum dots.

3.3. Biological properties

Impressive progress has been made in engineering bright CQDs bioprobes with good stability. However, biocompatibility of the functionalized CQDs is still a critical issue for further applications in live cells, tissues, and animals. Systematic cytotoxicity evaluations were carried out on both raw CQDs and passivated CQDs during the last few years. Sun's group employed CQDs produced by the arc-discharge of graphite rods, and then refluxed in HNO_3 for 12 h for cytotoxicity assay. The bare CQDs were apparently nontoxic to cells up to a relatively high concentration of 0.4 mg mL^{-1}. Luminescent CQDs synthesized by the electrochemical treatment of graphite were also evaluated in terms of cytotoxicity assay using a human kidney cell line, in which the cell viability was not affected by the dots.[19] Furthermore, Ray *et al.* improved a soot-based approach for CQDs synthesis with diameters of 26 nm.[91] The experimental results of cell viability also confirmed that the CQDs showed negligible cytotoxicity at concentrations required for fluorescence bioimaging.

The cytotoxicity of the CQDs passivated with functional groups, such as PEG,[26] PPEI-EI,[25] PEI,[92] BPEI (branched poly(ethylenimine)),[93] and PAA (poly(acrylic acid)),[94] were also evaluated in cytotoxicity assays. The PEGylated CQDs in all available configurations[27,95] were non-cytotoxic up to concentrations much higher than that is necessary for cell imaging and related applications. In addition, CQDs functionalized with PEG_{1500N} were injected into mice for toxicity evaluation up to 28 days, and the results suggested no significant toxic effects *in vivo*.[27] Moreover, experimental results indicated that the PPEI-EI-passivated CQDs were mostly nontoxic to the cells below a relatively high threshold of carbon core-equivalent PPEI-EI concentration.[25] According to the MTT assay, a PEI free sample was apparently nontoxic to HT-29 cells even at relatively high concentrations. However, the PEI-functionalized CQDs were more cytotoxic than PPEI-EI-functionalized CQDs. The more ethylenimine (EI) units within the PEI may be associated with the lower concentration thresholds for the CQDs to become cytotoxic, as PEI is the homopolymer corresponding to PPEI-EI with an extreme EI fraction of 100%. Free PAA in a nonaqueous solution was found to be harmful to cells even at relatively low

concentrations (50 μg mL^{-1}). The PAA-functionalized CQDs were generally comparable to free PAA at the same CQD core-equivalent concentrations, both were toxic to the cells with an exposure time of 24 h, but less so when the exposure time was shortened to 4 h. Overall, molecules with low cytotoxicity even at high concentrations such as PEG and PPEI-EI are suitable for CQDs functionalization for *in vivo* imaging and biosensing. Molecules with higher cytotoxicity including BPEI and PAA, can still be used to functionalize CQDs used *in vivo* if their concentrations are maintained low enough and the incubation time short enough.[92]

4. Applications

4.1. Biomedicine

4.1.1. Bioimaging. As fluorescent nanomaterials with biocompatibility and low biotoxicity, CQDs show great potential for fluorescent bioimaging,[25,26,40,96] and multimodal bioimaging of cells and tissues,[97] which have been reviewed elsewhere.[98–100]

The pioneering work on CQDs for bioimaging *in vitro*[2] and *in vivo*[26] was reported by Sun's group. Confocal microscopy images of *E. coli* ATCC 25922 labeled with the PEGylated CQDs were obtained at different excitation wavelengths. Yang *et al.* were the first to explore the feasibility of CQDs as a fluorescence contrast agent in mice.[27] In the experiments, PEGylated CQDs in an aqueous solution were injected subcutaneously into mice, and the fluorescence images at different excitation wavelengths collected. There was sufficient contrast for the imaging in both green and red emissions.[26] Tao *et al.* applied the same protocol to nude mice and obtained similar results.[101] More specifically, an aqueous solution of CQDs was injected subcutaneously into mice, followed by fluorescence imaging with excitations at seven different wavelengths from 455 nm to 704 nm. The best fluorescence contrast was obtained at an excitation of 595 nm (Fig. 20).

It is attractive to integrate multi-imaging technology for one agent for comprehensive understanding of the state of the illness. Most popular nanostructured multimodal imaging probes are combinations of magnetic resonance imaging (MRI) and optical imaging modalities. MRI can offer high spatial resolution and the capacity to simultaneously obtain physiological and anatomical information, whereas optical imaging allows for rapid screening.[102] Zboril *et al.* reported the synthesis of ultrafine Gd(III)-doped CQDs with a dual fluorescence/MRI character through the thermal decomposition of a precursor composed of an organic salt and a gadolinium(III) complex (Fig. 21).[97] The dots were water-dispersible, displaying bright fluorescence in the visible range upon light excitation, showing strong T1-weighted MRI contrast comparable to commercial Gadovist and possessing low cytotoxicity. In our opinion, it is possible to combine a common T1 MRI agent with CQDs *via* robust covalent bonding, which can increase the rotational correlation time (τ_R) of the T1-imaging probes.[103,104]

Srivastava *et al.* fabricated iron oxide-doped CQDs (IO-CQDs) for multi-modality (MR/fluorescence) bioimaging.[105] The IO-CQDs were prepared using the thermal decomposition of organic precursors in the presence of small Fe_3O_4 nanoparticles (with an average size of 6 nm). The IO-CQDs could be taken by RAW 264.7 cells, and the fluorescence was mainly detected in the cell cytoplasm. For *in vivo* imaging, the IO-CQDs were introduced into rats through intravenous injection. Fluorescence signals due to the IO-CQDs were observed in the spleen slide samples. The MRI results suggested enhanced signals in the brain blood vessel under both T1 and T2 models. It is also possible to combine other imaging technologies with the fluorescent imaging of CQDs for multi-modal bioimaging due to the biocompatibility of CQDs.

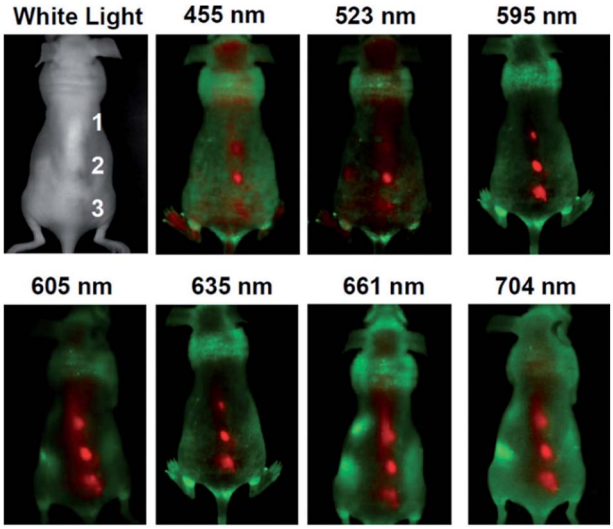

Fig. 20 *In vivo* fluorescence images of a CQDs-injected mice. The images were taken at various excitation wavelengths. Red and green represent fluorescent signals of the CQDs and the tissue auto-fluorescence, respectively. Adapted with permission.[101] Copyright 2012, Wiley-VCH.

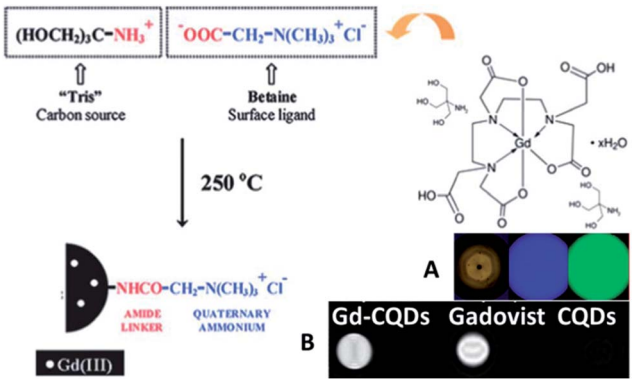

Fig. 21 Synthetic scheme for Gd-CQDs. (A) A brown aqueous dispersion of Gd-CQDs displays bright blue and green emission under 360–370 nm and 460–495 nm irradiation, respectively, (B) MRI positive contrast effects in T1-weighted images of Gd-CQDs, the commercial Gd-based contrast agent, *i.e.*, Gadovist (both samples were diluted in water with the same concentration of Gd), and undoped CQDs. All images were obtained using a 1.5 T clinical MRI tomograph. Adapted with permission.[97] Copyright 2012, Royal Society of Chemistry.

4.1.2. Biosensor. CQDs have been used as biosensor carriers for their high solubility in water, flexibility in surface modification, nontoxicity, excitation-dependent multicolor emission, excellent biocompatibility, good cell permeability, and high photostability. The CQDs-based biosensors can be used for visual monitoring of glucose,[106] cellular copper,[107] phosphate,[55] iron,[35] potassium,[108] pH,[109] and nucleic acid.[56]

CQDs can be used as an effective fluorescent sensing platform for nucleic acid detection with selectivity single-base mismatch. The general concept was based on the adsorption of the fluorescently labeled single-stranded DNA (ssDNA) probe by CQD *via* π–π interactions, which is accompanied by substantial fluorescence quenching, followed by specific hybridization with its target to form double-stranded DNA (dsDNA).[56] This results in desorption of the hybridized dsDNA from the CQD surface accompanied with subsequent recovery of fluorescence, probing the target DNA (Fig. 22).

A robust and multifunctional CQD-based fluorescence resonance energy transfer (FRET) probe for detecting and imaging mitochondrial H_2O_2 was demonstrated. The CQDs serve as the donor of energy transfer and the carrier for the sensing system. A boronate-based H_2O_2 recognition element, boronate-protected fluorescein (Fig. 23), was covalently linked onto the CQDs.[110] It can be used for tracking the exogenous H_2O_2 levels in L929 cells, and can also be used to visualize the endogenously produced H_2O_2 in RAW 264.7 macrophage cells.

4.1.3. Biomedicine delivery system. It is an attractive prospect to combine medical therapy and bioimaging diagnostics for visual drug distribution and monitoring of their effects.[111] A multifunctional theranostic agent (CD-Oxa) was prepared by the conjugation of an anticancer agent (oxidized oxaliplatin, oxa(IV)–COOH) onto the surface of CDs containing amine groups.[53] CD-Oxa successfully integrates the optical properties of the CDs and the therapeutic performance of Oxa. The *in vitro* results indicated that CD-Oxa possesses good biocompatibility, bioimaging function, and anticancer effects. The *in vivo* results demonstrate that it is possible to follow the track or distribution of the drug by monitoring the fluorescence signal of CD-Oxa, which helps customize the injection time and dosage of the medicine (Fig. 24A).

Kim *et al.* coupled CQDs with gold nanoparticles for an assembly, which was then conjugated with PEI–pDNA for delivering DNA to cells.[112] Note that fluorescence emissions from the assembly of CQD-gold nanoparticles could be quenched by pDNA; thus, the release of pDNA could be probed by the recovery of the fluorescence signals. The experimental results suggested that the assembly entered the cells with the CQDs located in the cell cytoplasm and the released pDNA entered the cell nuclei, achieving significant transfection efficiency (Fig. 24B). Pandey *et al.* used CQDs functionalized gold nanorods for the delivery of doxorubicin in a multi-modality fashion, including drug delivery, photothermal therapy, and bioimaging using the same platform.[113] The widely used anti-

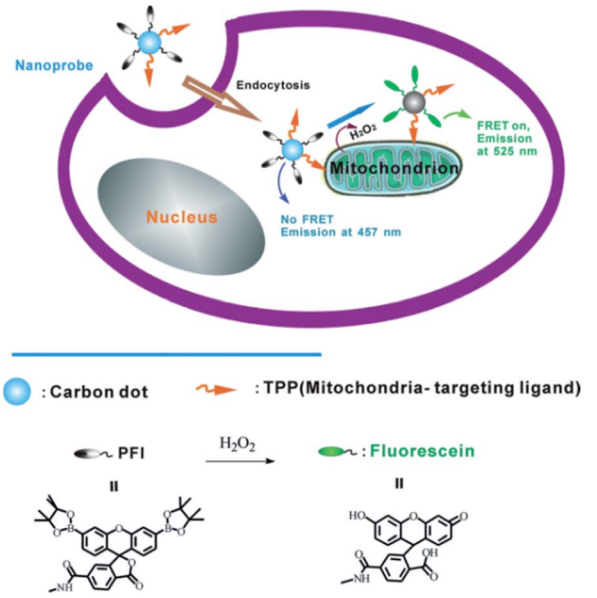

Fig. 23 Schematic illustration of FRET-based ratiometric sensing of mitochondrial H_2O_2 in living cells by the nanoprobe. Adapted with permission.[110] Copyright 2014, Wiley-VCH.

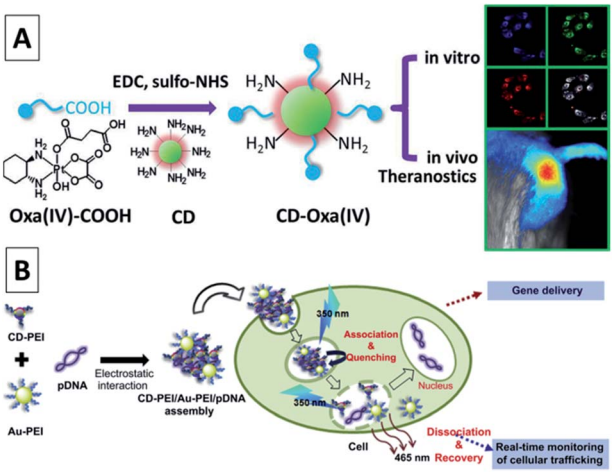

Fig. 24 (A) Synthetic scheme for CD-Oxa and its applications in bioimaging and theranostics. Adapted with permission.[53] Copyright 2014, Wiley-VCH. (B) A schematic illustration for the gene delivery and real-time monitoring of cellular trafficking utilizing CD-PEI/Au-PEI/pDNA assembled nanohybrids. Adapted with permission.[112] Copyright 2013, Elsevier.

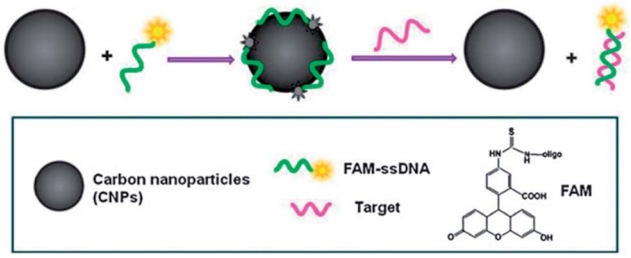

Fig. 22 A schematic (not to scale) illustrating the CQD-based fluorescent nucleic acid detection. Adapted with permission.[56] Copyright 2011, Royal Society of Chemistry.

psychotic drug haloperidol (HaLO)-grafted CQDs with cysteamine hydrochloride (CysHCl) as a linker can offer controlled release under physiological conditions for more than 40 h following the Hixson–Crowell model under standardized conditions.[114] A broad spectrum antibiotic, ciprofloxacin attached to CQDs with bright green fluorescence can not only pave a way for bioimaging but also provide an efficient new nanocarrier for controlled drug release with high antimicrobial activity under physiological conditions.[115]

4.2. Optronics

4.2.1. Dye-sensitized solar cells (DSCs). DSCs have aroused intense attention due to their diversity, low cost and easy processing. Though DSCs benefit from the diversity of organic dyes and get respectable efficiency, the photobleaching of organic dyes or the high cost and toxicity of ruthenium containing dyes, even the volatile electrolyte may hamper its widely application. CQDs with stable light absorption made from broad and cheap sources show its potential in DSCs.

After the first attempt by Ozin, who introduced CQDs as a sensitizer to capture sunlight in DSCs,[116] much research work has been performed to use this emergent nanolight to improve the performance of DSCs. As the charge recombination of photogenerated electrons in the porous electrode with either the oxidized dye or the electrolyte will reduce the efficiency of DSCs. Inspired by natural photosystems, Lee *et al.* developed a CQD-bridged dye/semiconductor complex system for the fabrication of highly efficient photoelectric conversion systems. CQDs not only enhanced the UV-vis absorbance of rhodamine B (RhB) solutions due to the synergistic hyperchromic effect between RhB and CQDs (Fig. 25), but also effectively suppressed the recombination of photogenerated electrons, thereby leading to a significantly enhanced photoelectric conversion efficiency.[117] Doping of CQDs into the dye/semiconductor complex significantly improved the photoelectric conversion efficiency of the complex by ~7 times.

4.2.2. Organic solar cells (OSCs). A simple and effective method to prepare CQDs and their polymer based composites was developed and the CQDs with an excitation wavelength independent PL can self-assemble in solution but not agglomerate in the solidified composite.[71] Accordingly, the composite with CQDs luminesce and exhibits a luminescent down-shifting (LDS) property. The P3HT:PCBM based solar cell harvests sunlight from 480 to 650 nm, only covering a part of visible light (380–780 nm) that contains the peak of the Sun's irradiance output. The remaining portions (380–480 nm and 650–780 nm) are not effectively utilized. Since the CQDs filled polysiloxane composite is able to emit light from 400 to 650 nm under excitation from 320 to 450 nm, its wavelength ranges of both PL and excitation well fit the harvesting spectrum (480–650 nm) and unused light spectrum (380–480 nm) of the bulk heterojunction (BHJ) solar cell. Because the emission wavelength range of the composite coincides with the response curve of the P3HT:PCBM-based BHJ solar cell, power conversion efficiency of the latter is raised by about 12% through coating a layer of the composite on the cover glass as a result of enhanced absorption of the near ultraviolet and blue-violet portions of sunlight (Fig. 26).

4.2.3. Supercapacitor. CQD-based hybrids as excellent electrode materials for supercapacitors were reported recently. The CQDs are fabricated by a facile chemical oxidation method followed by thermal reduction, and further decoration with RuO_2 to obtain the composites. The hybrid exhibits a specific capacitance of 460 F g^{-1} at an ultra-high current density of 50 A g^{-1} (41.9 wt% Ru loading), and excellent rate capability (88.6, 84.2, and 77.4% of capacity retention rate at 10, 20, and 50 A g^{-1} compared with 1 A g^{-1}, respectively).[118] Surprisingly, the hybrid shows exceptional cycling stability with 96.9% capacity retention over 5000 cycles at 5 A g^{-1}. Such remarkable electrochemical performance can be primarily ascribed to the significantly enhanced utilization of RuO_2 achieved by the efficient dispersion of small reduced CQDs, and the formation of a CQD-based hybrid network structure that can facilitate the fast charge transportation and ionic motion during the charge–discharge process. Moreover, the contact resistance at the interface between active materials and current collectors is determined to be a key factor in determining the performance

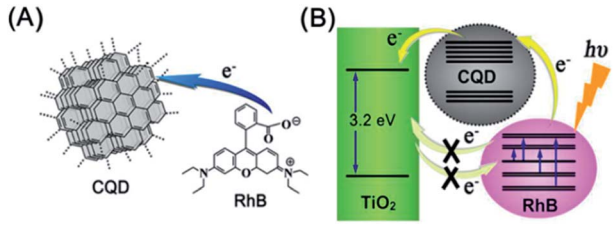

Fig. 25 (A) Scheme of electron transfer from RhB to CQDs. (B) CQDs serve as an electron transfer intermediary for bridging the photogenerated electrons and suppressing their recombination. Adapted with permission.[117] Copyright 2013, American Chemical Society.

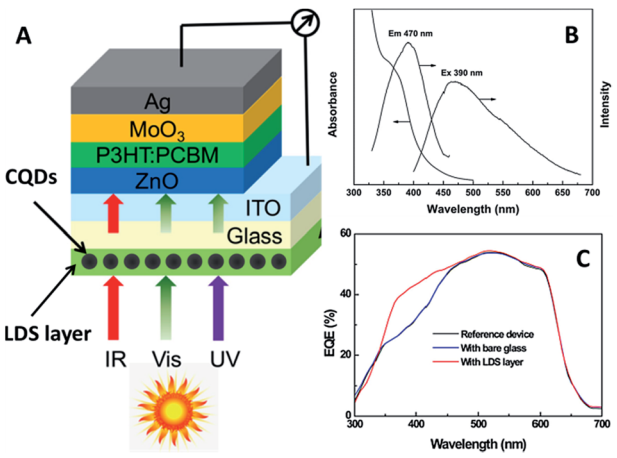

Fig. 26 (A) Schematic architecture of the BHJ solar cell with LDS layer. (B) UV-vis absorption and PL spectra of the CQDs filled polysiloxane composite (~20 μm thick) coated on glass. (C) Wavelength dependences of external quantum efficiency of the P3HT:PCBM-based solar cell with and without the LDS layer. Adapted with permission.[71] Copyright 2014, Elsevier.

of the hybrid (Fig. 27). CQDs-based ionic liquid (CQDIL) as a conductive agent and binder in an activated carbon electrode can improve supercapacitor performance due to the improved wettability of the electrolyte on the CQDIL-functionalized activated carbon electrode or a greater number of active components and a higher conductivity in the CQDIL/AC electrode. In addition, a high power density of 1.64 kW kg^{-1} and an ultra-high energy density of 83.2 W h kg^{-1} were obtained.[119]

4.2.4. Light-emitting devices (LED). CQDs are an emergent material for LEDs due to their stable light emitting, low cost and eco-friendliness.[47,120–124] Nitrogen-rich CQDs show broad and bright visible light under UV illumination that would be worth utilizing in phosphor applications.[123] Large-scale (20 × 20 cm) free-standing luminescent films of the CQDs embedded PMMA matrix were fabricated. The polymer matrix can not only provide mechanical support but also disperse the CQDs to prevent solid-state quenching. The obtained films are cost-effective, fully flexible, easily scalable, thermally stable, eco-friendly, and mechanically robust, and they show great potential in large-scale flexible solid-state lighting systems. White LEDs consist of the obtained films as the colour-converting phosphors and InGaN blue LEDs as the illuminators were also demonstrated. CQD-based LEDs with a driving current controlled colour change have been reported.[121] These devices consist of a CQD emissive layer sandwiched between an organic hole transport layer and an organic or inorganic electron transport layer (Fig. 28A) fabricated by a solution-based process. By tuning the device structure and the injecting current density (by changing the applied voltage), it is possible to obtain multicolour emission of blue, cyan, magenta, and white from the same CQDs (Fig. 28B). It is the first observation of switchable EL behaviour

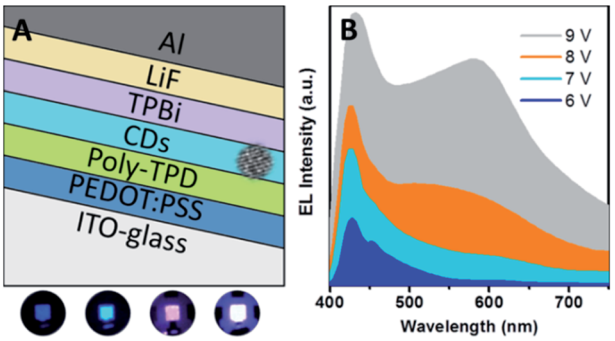

Fig. 28 (A) Sandwiched structure of LEDs using CQDs as a single emitting layer. (B) Electroluminescence (EL) spectra and true colour photographs of the blue, cyan, magenta, and white emissions. Adapted with permission.[121] Copyright 2013, American Chemical Society.

with white emission in single emitting layer structured nanomaterial LEDs. This interesting current density-dependent emission was useful for the development of colourful LEDs. The pure blue and white emissions were obtained by tuning the electron transport layer materials and the thickness of the electrode.

4.3. Catalysis

4.3.1. Photocatalysis. Advanced materials for electrocatalytic and photoelectrochemical (PEC) hydrogen evolution reaction (HER) are central to the area of renewable energy. CQDs-modified P25 TiO_2 composites (CQDs/P25) were prepared *via* a facile, one-step hydrothermal reaction.[125] CQDs/P25 exhibited improved photocatalytic H_2 evolution under irradiation with UV-Vis and visible light (λ > 450 nm) because of the CQDs acting as an electron reservoir to improve the efficient separation of the photoinduced electron–hole pairs of P25 and a photosensitizer to sensitize P25 into a visible light response structure for H_2 evolution.

It is expected to utilize the NIR region of sunlight for its large share of sun's energy. CQDs with the UCPL properties can improve the PEC properties of CQD/CdSe/TiO_2 NR photoanodes at the NIR region (over 750 nm) (Fig. 29).[126] The one-dimensional ordered TiO_2/CdSe core/shell heterostructural network (Fig. 29A) not only provides a large surface area for efficient

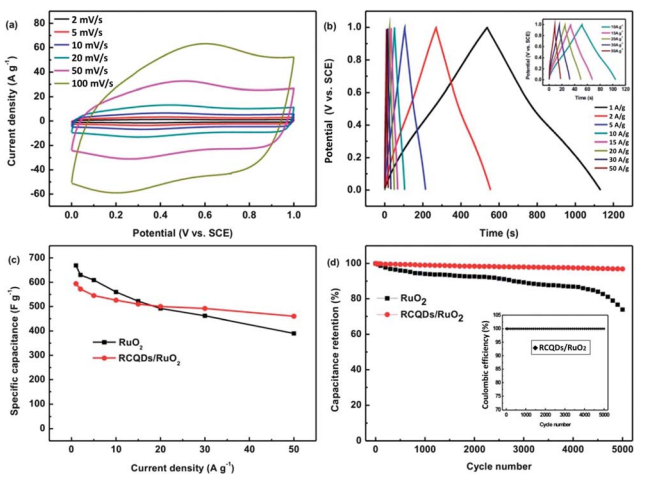

Fig. 27 (a) Cyclic voltammograms of RCQD/RuO_2 at different scan rates. (b) Charge–discharge curves of RCQD/RuO_2 at different current densities, and the inset shows a magnification at current densities of 10–50 A g^{-1}. (c) Comparison of the specific capacitance change of RuO_2 and RCQD/RuO_2 as a function of current density. (d) Comparison of the cycling stability of the RuO_2 and RCQD/RuO_2 at a current density of 5 A g^{-1}, and the inset shows the coulombic efficiency of RCQD/RuO_2. Adapted with permission.[118] Copyright 2013, Royal Society of Chemistry.

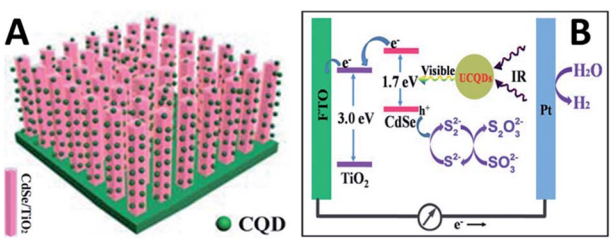

Fig. 29 (A) A schematic diagram showing the CQD/CdSe/TiO_2 NR photoanode. (B) A schematic diagram to illustrate how up-conversion of the carbon quantum dots (UCQDs) served as spectral converters for the CdSe/TiO_2 NR photoanode. Adapted with permission.[126] Copyright 2013, Royal Society of Chemistry.

loading of up-conversion CQDs, but also allows an excellent interfacial chemical reaction between the CdSe and electrolyte. Subsequently, CQDs were electrodeposited on the surface of the TiO_2/CdSe core/shell NRs to construct a CQD/CdSe/TiO_2 composite photoanode. Fig. 29B is the schematic diagram illustrating the whole PEC process under near-IR illumination. The CQDs can absorb near-IR photons and emit visible photons through the up-conversion effect to excite CdSe. Subsequently, the excited electrons in the conduction band of CdSe would rapidly inject into the conduction band of TiO_2, and then transfer along the axial direction of the TiO_2 NRs to the FTO substrate. The electrons would finally be transferred to the Pt counter electrode under the assistance of a little external bias voltage, and then drive the hydrogen evolution reaction. The holes remaining in the valence band of CdSe would be consumed by the sacrificial agent.

The oxygen reduction reaction (ORR) is another important photocatalytic reaction in many renewable-energy technologies, including fuel cells and water splitting.[127] The aggregates of nitrogen-doped CQDs from the hydrothermal treatment of natural willow leaves exhibit excellent electrocatalytic activity for the ORR *via* a dominant four-electron oxygen reduction pathway in 0.1 M KOH aqueous solution, great stability (even after 20 000 cycles), as well as methanol and CO tolerance superior to a commercial Pt/C catalyst.[128] The heteroatom-doped carbon materials not only exhibit good electrochemical activity for the ORR, but also excellent stability and immunity towards methanol and CO in practical applications, which is one of the main challenges that metal-based catalysts are facing.

4.3.2. Other catalysis. A facile and green approach was reported to synthesize bifunctional fluorescent nitrogen-doped CQDs *via* the one-step hydrothermal treatment of soy milk at 180 °C, which not only showed favorable photoluminescent properties, but also exhibited good electrocatalytic activity towards ORR.[129] The number of electrons involved in the overall ORR was calculated to be 3.15 at −1.20 V, indicating that a four-electron pathway and a two-electron transfer pathway occurred simultaneously.

Dey *et al.* showed the fabrication of CQDs from a bio-precursor and used them for the reduction of $PdCl_4^{2-}$ salts leading to the formation of Pd@CQD core–shell nanostructures.[130] Although bare CQDs were not capable of preventing the agglomeration of the Pd NPs during the Suzuki and Heck reactions, addition of a co-stabilizer in the form of poly-(*N*-vinyl-2-pyrrolidone) (PVP) led to an efficient composite that showed high catalytic activity towards the formation of C–C bonds. The Pd@CQD-PVP catalysts were reused in subsequent reactions and the results showed efficient catalytic activity after the third cycle even with obvious structural changes.

4.4. Chemical sensors

By monitoring the changes in their fluorescence intensity under external physical or chemical stimuli, CQDs were used to detect substances and quantities such as DNA,[56] PO_4^{3-},[55] thrombin,[131] nitrite,[132] glucose,[106] biothiol,[133] Fe^{3+},[134] pH,[62] Ag^+,[135] Hg^{2+},[133,136] and Cu^{2+}.[137,138]

Qu *et al.* reported a preparative route toward distinctive fluorescent CQDs from dopamine (DA). Such CQDs exhibit excellent PL properties, and they can be used for multicolour bioimaging. More importantly, these CQDs were used as a new type of sensor for label-free detection of Fe^{3+} and dopamine (DA) with high sensitivity and selectivity.[61] The method relies on the fact that Fe^{3+} can oxidize the hydroquinone groups on the surfaces of CQDs to the quinone species, which can quench the fluorescence of the CQDs and DA can effectively shelter the fluorescence quenching due to their competition with CQDs to react with Fe^{3+} (Fig. 30). It offers a convenient "mix-and-detect" protocol for rapid detection of Fe^{3+} and DA and can be easily accomplished with a rapid one-step (within 10 min) operation. Moreover, this sensing platform exhibits high sensitivity and selectivity toward Fe^{3+} and DA *versus* other metal ions and the other DA analogues. Furthermore, no further chemical modification of the CQDs was required, which offers the advantages of simplicity and cost efficiency. More importantly, the new strategy eliminates the need of QDs, organic dyes, and/or organic solvents, showing much more environmentally friendliness.

A FRET ratiometric fluorescent sensor was developed for detecting H_2S in aqueous media and serum over a wide pH range of 4.0–9.0, as well as inside live cells. In the sensing system, upon being reduced by H_2S, the probe turns into an energy acceptor (naphthalimide–amine), and accordingly exhibits an absorption at around 425 nm and emission at about 526 nm.[139] The fluorescence change of the sensor upon addition of H_2S was measured and established a working curve by plotting the emission intensity ratio (I_{526}/I_{425}) *versus* H_2S concentration (Fig. 31A). It can be seen that, in the absence of H_2S, the excitation of CQDs at 340 nm led to emission of CQDs at 425 nm; moreover, with the addition of H_2S, the CQD emission at 425 nm gradually decreased, and a new emission band at 526 nm appeared, corresponding to the fluorescence of naphthalimide–amine. In the presence of H_2S, the probe

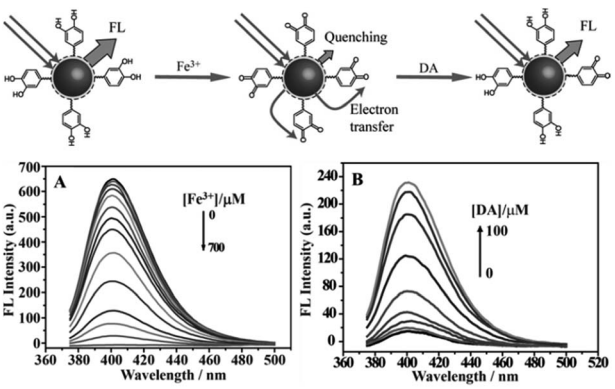

Fig. 30 (Up) Schematic representation of fluorescent CQDs for the detection of Fe^{3+} ions and dopamine. (A) Representative fluorescence emission spectra of CQDs in the presence of increasing Fe^{3+} concentration (0–700 μM) in a HEPES buffer (10 mM) at pH 7.0. (B) Fluorescence emission spectra of CQDs containing Fe^{3+} (600 μM) with increase in DA concentration (0–100 μM). Adapted with permission.[61] Copyright 2013, Wiley-VCH.

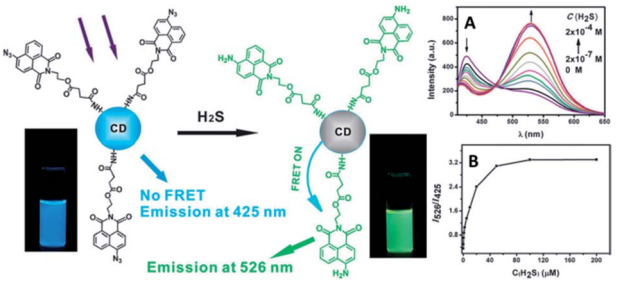

Fig. 31 (Left) Schematic illustration for the structure of the CQD-based sensor and its ratiometric detection of H_2S. Photographs were obtained under a hand-held UV lamp. (Right) (A) Fluorescence spectra of the CQD-based sensor (concentration: 0.45 mg mL^{-1}) in the presence of different amounts of H_2S; (B) fluorescence intensity ratio of the CQD-based sensor as a function of H_2S concentration in HEPES buffered (pH 7.4) water–ethanol (3 : 1, v/v) (λ_{exc} = 340 nm). Adapted with permission.[139] Copyright 2013, Royal Society of Chemistry.

(naphthalimide–azide) changed into an energy acceptor (naphthalimide–amine) due to its reduction by H_2S. From Fig. 31B, it is clear that the fluorescence ratio (I_{526}/I_{425}) increases gradually with an increase in H_2S concentration. Furthermore, the fluorescence of the suspension also became bright green upon addition of H_2S. By adjusting the amount of the probe moieties coupled onto the CQD, the detection limit can reach 10 nM, which is the lowest among fluorescent sensors for H_2S.

5. Summary and outlook

In this feature article, we have described the recent progress in the field of CQDs, focusing on their synthetic methods, size control, modification strategies, PL properties, luminescent mechanism, and applications in biomedicine, energy conversion and storage, catalysis, and sensor issues.

Though several methods have been proposed towards the synthesis of CQDs, well-defined structure and precise sizes are hardly available yet. It is critical to synthesize CQDs in a facile and green manner with designed structure and size for property studies and selected applications.

The explored properties of CQDs and their regulations are fascinating for extensive applications in science, which have been demonstrated. New properties and how to subtly tune these properties, such as fresh phosphorescence and debatable UCPL, are also challengeable for its nubilous luminescent mechanism. The amorphous to nearly crystalline internal structure, nonquantitative surface structure and virtual size polydispersion may block the clarification of the luminescence mechanism. This problem will be solved through the accurate synthesis, careful analysis, and intelligent consideration.

Many studies have demonstrated the CQDs' versatility in biomedicine: (i) multimodal bioimaging for its flexibility in surface modification to combine other imaging agents for its high biocompatibility, (ii) biosensors for its multi stimulus responses, (iii) delivery carrier for its various combination with biomolecules or drugs *via* multi reaction and stimulus responses.

It will arouse research interest in using CQDs in optronics, including photovoltaic conversion, photochemical transformation and energy storage, for the optical properties of CQDs such as electroluminescence, down- and up-conversion, as well as its dual role as electron donor and acceptor with good conductivity and distribution.

Acknowledgements

The support of the National Natural Science Foundation of China (20874026, 91023008, 21274042), the Ph.D. Programs Foundation of Ministry of Education of China (20100074110002), the Fundamental Research Funds for the Central Universities, and the Shanghai Leading Academic Discipline Project (B502) is gratefully acknowledged.

Notes and references

1 X. Xu, R. Ray, Y. Gu, H. J. Ploehn, L. Gearheart, K. Raker and W. A. Scrivens, *J. Am. Chem. Soc.*, 2004, **126**, 12736.
2 Y.-P. Sun, B. Zhou, Y. Lin, W. Wang, K. S. Fernando, P. Pathak, M. J. Meziani, B. A. Harruff, X. Wang and H. Wang, *J. Am. Chem. Soc.*, 2006, **128**, 7756.
3 S. N. Baker and G. A. Baker, *Angew. Chem., Int. Ed.*, 2010, **49**, 6726.
4 H. Li, Z. Kang, Y. Liu and S.-T. Lee, *J. Mater. Chem.*, 2012, **22**, 24230.
5 J. Shen, Y. Zhu, X. Yang and C. Li, *Chem. Commun.*, 2012, **48**, 3686.
6 L. Li, G. Wu, G. Yang, J. Peng, J. Zhao and J.-J. Zhu, *Nanoscale*, 2013, **5**, 4015.
7 Z. Zhang, J. Zhang, N. Chen and L. Qu, *Energy Environ. Sci.*, 2012, **5**, 8869.
8 B. Zhu, S. Sun, Y. Wang, S. Deng, G. Qian, M. Wang and A. Hu, *J. Mater. Chem. C*, 2013, **1**, 580.
9 S. Ray, A. Saha, N. R. Jana and R. Sarkar, *J. Phys. Chem. C*, 2009, **113**, 18546.
10 L. Tian, D. Ghosh, W. Chen, S. Pradhan, X. Chang and S. Chen, *Chem. Mater.*, 2009, **21**, 2803.
11 Z.-A. Qiao, Y. Wang, Y. Gao, H. Li, T. Dai, Y. Liu and Q. Huo, *Chem. Commun.*, 2010, **46**, 8812.
12 Y. Dong, N. Zhou, X. Lin, J. Lin, Y. Chi and G. Chen, *Chem. Mater.*, 2010, **22**, 5895.
13 H. Peng and J. Travas-Sejdic, *Chem. Mater.*, 2009, **21**, 5563.
14 L. Shen, L. Zhang, M. Chen, X. Chen and J. Wang, *Carbon*, 2013, **55**, 343.
15 J. Zhou, C. Booker, R. Li, X. Zhou, T.-K. Sham, X. Sun and Z. Ding, *J. Am. Chem. Soc.*, 2007, **129**, 744.
16 D. B. Shinde and V. K. Pillai, *Chem.–Eur. J.*, 2012, **18**, 12522.
17 L. Bao, Z. L. Zhang, Z. Q. Tian, L. Zhang, C. Liu, Y. Lin, B. Qi and D. W. Pang, *Adv. Mater.*, 2011, **23**, 5801.
18 L. Zheng, Y. Chi, Y. Dong, J. Lin and B. Wang, *J. Am. Chem. Soc.*, 2009, **131**, 4564.
19 Q.-L. Zhao, Z.-L. Zhang, B.-H. Huang, J. Peng, M. Zhang and D.-W. Pang, *Chem. Commun.*, 2008, 5116, DOI: 10.1039/b812420e.

20 H. Ming, Z. Ma, Y. Liu, K. Pan, H. Yu, F. Wang and Z. Kang, *Dalton Trans.*, 2012, **41**, 9526.
21 H. Li, X. He, Z. Kang, H. Huang, Y. Liu, J. Liu, S. Lian, C. H. A. Tsang, X. Yang and S. T. Lee, *Angew. Chem., Int. Ed.*, 2010, **49**, 4430.
22 J. Deng, Q. Lu, N. Mi, H. Li, M. Liu, M. Xu, L. Tan, Q. Xie, Y. Zhang and S. Yao, *Chem.–Eur. J.*, 2014, **20**, 4993.
23 S.-L. Hu, K.-Y. Niu, J. Sun, J. Yang, N.-Q. Zhao and X.-W. Du, *J. Mater. Chem.*, 2009, **19**, 484.
24 X. Li, H. Wang, Y. Shimizu, A. Pyatenko, K. Kawaguchi and N. Koshizaki, *Chem. Commun.*, 2011, **47**, 932.
25 L. Cao, X. Wang, M. J. Meziani, F. Lu, H. Wang, P. G. Luo, Y. Lin, B. A. Harruff, L. M. Veca and D. Murray, *J. Am. Chem. Soc.*, 2007, **129**, 11318.
26 S.-T. Yang, L. Cao, P. G. Luo, F. Lu, X. Wang, H. Wang, M. J. Meziani, Y. Liu, G. Qi and Y.-P. Sun, *J. Am. Chem. Soc.*, 2009, **131**, 11308.
27 S.-T. Yang, X. Wang, H. Wang, F. Lu, P. G. Luo, L. Cao, M. J. Meziani, J.-H. Liu, Y. Liu and M. Chen, *J. Phys. Chem. C*, 2009, **113**, 18110.
28 H. Zhu, X. Wang, Y. Li, Z. Wang, F. Yang and X. Yang, *Chem. Commun.*, 2009, 5118.
29 X. Zhai, P. Zhang, C. Liu, T. Bai, W. Li, L. Dai and W. Liu, *Chem. Commun.*, 2012, **48**, 7955.
30 Y. Liu, N. Xiao, N. Gong, H. Wang, X. Shi, W. Gu and L. Ye, *Carbon*, 2014, **68**, 258.
31 A. Jaiswal, S. S. Ghosh and A. Chattopadhyay, *Chem. Commun.*, 2012, **48**, 407.
32 B. Hu, K. Wang, L. Wu, S. H. Yu, M. Antonietti and M. M. Titirici, *Adv. Mater.*, 2010, **22**, 813.
33 M.-M. Titirici and M. Antonietti, *Chem. Soc. Rev.*, 2010, **39**, 103.
34 Z.-C. Yang, M. Wang, A. M. Yong, S. Y. Wong, X.-H. Zhang, H. Tan, A. Y. Chang, X. Li and J. Wang, *Chem. Commun.*, 2011, **47**, 11615.
35 S. Zhu, Q. Meng, L. Wang, J. Zhang, Y. Song, H. Jin, K. Zhang, H. Sun, H. Wang and B. Yang, *Angew. Chem., Int. Ed.*, 2013, **125**, 4045.
36 Y. Yang, J. Cui, M. Zheng, C. Hu, S. Tan, Y. Xiao, Q. Yang and Y. Liu, *Chem. Commun.*, 2012, **48**, 380.
37 B. De and N. Karak, *RSC Adv.*, 2013, **3**, 8286.
38 Z. Zhang, J. Hao, J. Zhang, B. Zhang and J. Tang, *RSC Adv.*, 2012, **2**, 8599.
39 S. Sahu, B. Behera, T. K. Maiti and S. Mohapatra, *Chem. Commun.*, 2012, **48**, 8835.
40 S. K. Bhunia, A. Saha, A. R. Maity, S. C. Ray and N. R. Jana, *Sci. Rep.*, 2013, **3**, 1473.
41 Y. Xu, M. Wu, Y. Liu, X. Z. Feng, X. B. Yin, X. W. He and Y. K. Zhang, *Chem.–Eur. J.*, 2013, **19**, 2276.
42 Y. Wang, L. Dong, R. Xiong and A. Hu, *J. Mater. Chem. C*, 2013, **1**, 7731.
43 A. B. Bourlinos, A. Stassinopoulos, D. Anglos, R. Zboril, V. Georgakilas and E. P. Giannelis, *Chem. Mater.*, 2008, **20**, 4539.
44 R. Liu, D. Wu, S. Liu, K. Koynov, W. Knoll and Q. Li, *Angew. Chem., Int. Ed.*, 2009, **48**, 4598.
45 J. Zong, Y. Zhu, X. Yang, J. Shen and C. Li, *Chem. Commun.*, 2011, **47**, 764.
46 C. Tang, K. Qi, K. L. Wooley, K. Matyjaszewski and T. Kowalewski, *Angew. Chem., Int. Ed.*, 2004, **116**, 2843.
47 X. Guo, C.-F. Wang, Z.-Y. Yu, L. Chen and S. Chen, *Chem. Commun.*, 2012, **48**, 2692.
48 M. E. Mackay, A. Tuteja, P. M. Duxbury, C. J. Hawker, B. Van Horn, Z. Guan, G. Chen and R. Krishnan, *Science*, 2006, **311**, 1740.
49 Y. Xiao and A. Hu, *Macromol. Rapid Commun.*, 2011, **32**, 1688.
50 B. Zhu, J. Ma, Z. Li, J. Hou, X. Cheng, G. Qian, P. Liu and A. Hu, *J. Mater. Chem.*, 2011, **21**, 2679.
51 B. Zhu, G. Qian, Y. Xiao, S. Deng, M. Wang and A. Hu, *J. Polym. Sci., Part A: Polym. Chem.*, 2011, **49**, 5330.
52 J.-Y. Yin, H.-J. Liu, S. Jiang, Y. Chen and Y. Yao, *ACS Macro Lett.*, 2013, **2**, 1033.
53 M. Zheng, S. Liu, J. Li, D. Qu, H. Zhao, X. Guan, X. Hu, Z. Xie, X. Jing and Z. Sun, *Adv. Mater.*, 2014, **26**, 3554.
54 Y. Dong, R. Wang, H. Li, J. Shao, Y. Chi, X. Lin and G. Chen, *Carbon*, 2012, **50**, 2810.
55 H. X. Zhao, L. Q. Liu, Z. De Liu, Y. Wang, X. J. Zhao and C. Z. Huang, *Chem. Commun.*, 2011, **47**, 2604.
56 H. Li, Y. Zhang, L. Wang, J. Tian and X. Sun, *Chem. Commun.*, 2011, **47**, 961.
57 F. Wang, Z. Xie, H. Zhang, C. y. Liu and Y. g. Zhang, *Adv. Funct. Mater.*, 2011, **21**, 1027.
58 Y. Mao, Y. Bao, D. Han, F. Li and L. Niu, *Biosens. Bioelectron.*, 2012, **38**, 55.
59 B. Liao, P. Long, B. He, S. Yi, B. Ou, S. Shen and J. Chen, *J. Mater. Chem. C*, 2013, **1**, 3716.
60 J. Zhou, Y. Yang and C.-y. Zhang, *Chem. Commun.*, 2013, **49**, 8605.
61 K. Qu, J. Wang, J. Ren and X. Qu, *Chem.–Eur. J.*, 2013, **19**, 7243.
62 M. J. Krysmann, A. Kelarakis, P. Dallas and E. P. Giannelis, *J. Am. Chem. Soc.*, 2011, **134**, 747.
63 D. Sun, R. Ban, P.-H. Zhang, G.-H. Wu, J.-R. Zhang and J.-J. Zhu, *Carbon*, 2013, **64**, 424.
64 S. Chandra, P. Patra, S. H. Pathan, S. Roy, S. Mitra, A. Layek, R. Bhar, P. Pramanik and A. Goswami, *J. Mater. Chem. B*, 2013, **1**, 2375.
65 K. S. Prasad, R. Pallela, D. M. Kim and Y. B. Shim, *Part. Part. Syst. Charact.*, 2013, **30**, 557.
66 P. Ayala, R. Arenal, A. Loiseau, A. Rubio and T. Pichler, *Rev. Mod. Phys.*, 2010, **82**, 1843.
67 F. Li, C. Liu, J. Yang, Z. Wang, W. Liu and F. Tian, *RSC Adv.*, 2014, **4**, 3201.
68 H. Zhang, H. Ming, S. Lian, H. Huang, H. Li, L. Zhang, Y. Liu, Z. Kang and S.-T. Lee, *Dalton Trans.*, 2011, **40**, 10822.
69 J. Wang, M. Gao and G. W. Ho, *J. Mater. Chem. A*, 2014, **2**, 5703.
70 J. Zong, X. Yang, A. Trinchi, S. Hardin, I. Cole, Y. Zhu, C. Li, T. Muster and G. Wei, *Nanoscale*, 2013, **5**, 11200.
71 J. J. Huang, Z. F. Zhong, M. Z. Rong, X. Zhou, X. D. Chen and M. Q. Zhang, *Carbon*, 2014, **70**, 190.

72 Y. Deng, D. Zhao, X. Chen, F. Wang, H. Song and D. Shen, *Chem. Commun.*, 2013, **49**, 5751.
73 Z. Lin, W. Xue, H. Chen and J.-M. Lin, *Chem. Commun.*, 2012, **48**, 1051.
74 P. Teng, J. Xie, Y. Long, X. Huang, R. Zhu, X. Wang, L. Liang, Y. Huang and H. Zheng, *J. Lumin.*, 2014, **146**, 464.
75 X. Dou, Z. Lin, H. Chen, Y. Zheng, C. Lu and J.-M. Lin, *Chem. Commun.*, 2013, **49**, 5871.
76 L. Zhao, F. Di, D. Wang, L.-H. Guo, Y. Yang, B. Wan and H. Zhang, *Nanoscale*, 2013, **5**, 2655.
77 J. Shi, C. Lu, D. Yan and L. Ma, *Biosens. Bioelectron.*, 2013, **45**, 58.
78 Y. Xu, M. Wu, X. Z. Feng, X. B. Yin, X. W. He and Y. K. Zhang, *Chem.–Eur. J.*, 2013, **19**, 6282.
79 X. Jia, J. Li and E. Wang, *Nanoscale*, 2012, **4**, 5572.
80 X. Wen, P. Yu, Y.-R. Toh, X. Ma and J. Tang, *Chem. Commun.*, 2014, **50**, 4703.
81 X. Wang, L. Cao, F. Lu, M. J. Meziani, H. Li, G. Qi, B. Zhou, B. A. Harruff, F. Kermarrec and Y.-P. Sun, *Chem. Commun.*, 2009, 3774.
82 J. Xu, S. Sahu, L. Cao, C. E. Bunker, G. Peng, Y. Liu, K. S. Fernando, P. Wang, E. A. Guliants and M. J. Meziani, *Langmuir*, 2012, **28**, 16141.
83 P. Yu, X. Wen, Y.-R. Toh, Y.-C. Lee, K.-Y. Huang, S. Huang, S. Shrestha, G. Conibeer and J. Tang, *J. Mater. Chem. C*, 2014, **2**, 2894.
84 Y. Fang, S. Guo, D. Li, C. Zhu, W. Ren, S. Dong and E. Wang, *ACS Nano*, 2011, **6**, 400.
85 X.-J. Mao, H.-Z. Zheng, Y.-J. Long, J. Du, J.-Y. Hao, L.-L. Wang and D.-B. Zhou, *Spectrochim. Acta, Part A*, 2009, **75**, 553.
86 A. B. Bourlinos, R. Zbořil, J. Petr, A. Bakandritsos, M. Krysmann and E. P. Giannelis, *Chem. Mater.*, 2011, **24**, 6.
87 S. Srivastava and N. S. Gajbhiye, *ChemPhysChem*, 2011, **12**, 2624.
88 S. K. Das, Y. Liu, S. Yeom, D. Y. Kim and C. I. Richards, *Nano Lett.*, 2014, **14**, 620.
89 H. Zheng, Q. Wang, Y. Long, H. Zhang, X. Huang and R. Zhu, *Chem. Commun.*, 2011, **47**, 10650.
90 L. Wang, S.-J. Zhu, H.-Y. Wang, S.-N. Qu, Y.-L. Zhang, J.-H. Zhang, Q.-D. Chen, H.-L. Xu, W. Han and B. Yang, *ACS Nano*, 2014, **8**, 2541.
91 S. C. Ray, A. Saha, N. R. Jana and R. Sarkar, *J. Phys. Chem. C*, 2009, **113**, 18546.
92 Y. Wang, P. Anilkumar, L. Cao, J.-H. Liu, P. G. Luo, K. N. Tackett, S. Sahu, P. Wang, X. Wang and Y.-P. Sun, *Exp. Biol. Med.*, 2011, **236**, 1231.
93 Y. Dong, R. Wang, G. Li, C. Chen, Y. Chi and G. Chen, *Anal. Chem.*, 2012, **84**, 6220.
94 Y. Wang, L. Bao, Z. Liu and D.-W. Pang, *Anal. Chem.*, 2011, **83**, 8130.
95 X. Wang, L. Cao, S. T. Yang, F. Lu, M. J. Meziani, L. Tian, K. W. Sun, M. A. Bloodgood and Y. P. Sun, *Angew. Chem., Int. Ed.*, 2010, **122**, 5438.
96 B. Chen, F. Li, S. Li, W. Weng, H. Guo, T. Guo, X. Zhang, Y. Chen, T. Huang and X. Hong, *Nanoscale*, 2013, **5**, 1967.
97 A. B. Bourlinos, A. Bakandritsos, A. Kouloumpis, D. Gournis, M. Krysmann, E. P. Giannelis, K. Polakova, K. Safarova, K. Hola and R. Zboril, *J. Mater. Chem.*, 2012, **22**, 23327.
98 P. G. Luo, S. Sahu, S.-T. Yang, S. K. Sonkar, J. Wang, H. Wang, G. E. LeCroy, L. Cao and Y.-P. Sun, *J. Mater. Chem. B*, 2013, **1**, 2116.
99 P. G. Luo, F. Yang, S.-T. Yang, S. K. Sonkar, L. Yang, J. J. Broglie, Y. Liu and Y.-P. Sun, *RSC Adv.*, 2014, **4**, 10791.
100 C. Ding, A. Zhu and Y. Tian, *Acc. Chem. Res.*, 2013, **47**, 20.
101 H. Tao, K. Yang, Z. Ma, J. Wan, Y. Zhang, Z. Kang and Z. Liu, *Small*, 2012, **8**, 281.
102 D.-E. Lee, H. Koo, I.-C. Sun, J. H. Ryu, K. Kim and I. C. Kwon, *Chem. Soc. Rev.*, 2009, **41**, 2656.
103 P. Gong, Z. Chen, Y. Chen, W. Wang, X. Wang and A. Hu, *Chem. Commun.*, 2011, **47**, 4240.
104 Y. Chen, H. Yang, W. Tang, X. Cui, W. Wang, X. Chen, Y. Yuan and A. Hu, *J. Mater. Chem. B*, 2013, **1**, 5443.
105 S. Srivastava, R. Awasthi, D. Tripathi, M. K. Rai, V. Agarwal, V. Agrawal, N. S. Gajbhiye and R. K. Gupta, *Small*, 2012, **8**, 1099.
106 W. Shi, Q. Wang, Y. Long, Z. Cheng, S. Chen, H. Zheng and Y. Huang, *Chem. Commun.*, 2011, **47**, 6695.
107 A. Zhu, Q. Qu, X. Shao, B. Kong and Y. Tian, *Angew. Chem., Int. Ed.*, 2012, **124**, 7297.
108 W. Wei, C. Xu, J. Ren, B. Xu and X. Qu, *Chem. Commun.*, 2012, **48**, 1284.
109 W. Shi, X. Li and H. Ma, *Angew. Chem., Int. Ed.*, 2012, **51**, 6432.
110 F. Du, Y. Min, F. Zeng, C. Yu and S. Wu, *Small*, 2014, **10**, 964.
111 Z. Cheng, A. Al Zaki, J. Z. Hui, V. R. Muzykantov and A. Tsourkas, *Science*, 2012, **338**, 903.
112 J. Kim, J. Park, H. Kim, K. Singha and W. J. Kim, *Biomaterials*, 2013, **34**, 7168.
113 S. Pandey, M. Thakur, A. Mewada, D. Anjarlekar, N. Mishra and M. Sharon, *J. Mater. Chem. B*, 2013, **1**, 4972.
114 S. Pandey, A. Mewada, M. Thakur, A. Tank and M. Sharon, *RSC Adv.*, 2013, **3**, 26290.
115 M. Thakur, S. Pandey, A. Mewada, V. Patil, M. Khade, E. Goshi and M. Sharon, *J. Drug Delivery*, 2014, **2014**, 282193.
116 P. Mirtchev, E. J. Henderson, N. Soheilnia, C. M. Yip and G. A. Ozin, *J. Mater. Chem.*, 2012, **22**, 1265.
117 Z. Ma, Y.-L. Zhang, L. Wang, H. Ming, H. Li, X. Zhang, F. Wang, Y. Liu, Z. Kang and S.-T. Lee, *ACS Appl. Mater. Interfaces*, 2013, **5**, 5080.
118 Y. Zhu, X. Ji, C. Pan, Q. Sun, W. Song, L. Fang, Q. Chen and C. E. Banks, *Energy Environ. Sci.*, 2013, **6**, 3665.
119 Y. Wei, H. Liu, Y. Jin, K. Cai, H. Li, Y. Liu, Z. Kang and Q. Zhang, *New J. Chem.*, 2013, **37**, 886.
120 W. Kwon, S. Do, D. C. Won and S.-W. Rhee, *ACS Appl. Mater. Interfaces*, 2013, **5**, 822.
121 X. Zhang, Y. Zhang, Y. Wang, S. Kalytchuk, S. V. Kershaw, Y. Wang, P. Wang, T. Zhang, Y. Zhao and H. Zhang, *ACS Nano*, 2013, **7**, 11234.

122 L. Mao, W.-Q. Tang, Z.-Y. Deng, S.-S. Liu, C.-F. Wang and S. Chen, *Ind. Eng. Chem. Res.*, 2014, **53**, 6417.
123 W. Kwon, S. Do, J. Lee, S. Hwang, J. K. Kim and S.-W. Rhee, *Chem. Mater.*, 2013, **25**, 1893.
124 F. Wang, Y.-h. Chen, C.-y. Liu and D.-g. Ma, *Chem. Commun.*, 2011, **47**, 3502.
125 H. Yu, Y. Zhao, C. Zhou, L. Shang, Y. Peng, Y. Cao, L.-Z. Wu, C.-H. Tung and T. Zhang, *J. Mater. Chem. A*, 2014, **2**, 3344.
126 X. Zhang, H. Huang, J. Liu, Y. Liu and Z. Kang, *J. Mater. Chem. A*, 2013, **1**, 11529.
127 Y. Liang, Y. Li, H. Wang, J. Zhou, J. Wang, T. Regier and H. Dai, *Nat. Mater.*, 2011, **10**, 780.
128 S. Gao, Y. Chen, H. Fan, X. Wei, C. Hu, L. Wang and L. Qu, *J. Mater. Chem. A*, 2014, **2**, 6320.
129 C. Zhu, J. Zhai and S. Dong, *Chem. Commun.*, 2012, **48**, 9367.
130 D. Dey, T. Bhattacharya, B. Majumdar, S. Mandani, B. Sharma and T. K. Sarma, *Dalton Trans.*, 2013, **42**, 13821.
131 J. Liu, J. Li, Y. Jiang, S. Yang, W. Tan and R. Yang, *Chem. Commun.*, 2011, **47**, 11321.
132 Z. Lin, W. Xue, H. Chen and J.-M. Lin, *Anal. Chem.*, 2011, **83**, 8245.
133 L. Zhou, Y. Lin, Z. Huang, J. Ren and X. Qu, *Chem. Commun.*, 2012, **48**, 1147.
134 S. Qu, H. Chen, X. Zheng, J. Cao and X. Liu, *Nanoscale*, 2013, **5**, 5514.
135 H. Li, J. Zhai and X. Sun, *Langmuir*, 2011, **27**, 4305.
136 H. Li, J. Zhai, J. Tian, Y. Luo and X. Sun, *Biosens. Bioelectron.*, 2011, **26**, 4656.
137 S. Liu, J. Tian, L. Wang, Y. Zhang, X. Qin, Y. Luo, A. M. Asiri, A. O. Al-Youbi and X. Sun, *Adv. Mater.*, 2012, **24**, 2037.
138 Q. Qu, A. Zhu, X. Shao, G. Shi and Y. Tian, *Chem. Commun.*, 2012, **48**, 5473.
139 C. Yu, X. Li, F. Zeng, F. Zheng and S. Wu, *Chem. Commun.*, 2013, **49**, 403.